Calculation method of mesh stiffness for helical gear pair with manufacturing errors, assembly errors and tooth modifications

Chang Liu [ID] · **Wankai Shi** [ID] · **Kun Liu** [ID]

Abstract For the accurate calculation of the time-varying mesh stiffness (TVMS) of helical gear pairs, a novel method is proposed in this paper. This proposed method can predict the TVMS based on the gear accuracy grade or the measurement coordinates of the tooth surface. The abnormal meshing phenomena caused by manufacturing errors (MEs), assembly errors (AEs), and tooth modifications (TMs), such as the loss of contact of tooth pairs, out-of-line meshing, and eccentric loads, are considered in the calculation process. The proposed method was verified to be effective for both spur and helical gear pairs. The effects of MEs, AEs, and TMs on the TVMS of helical gear pairs were also investigated. The results showed that the pitch, helix, and misalignment deviations were the main influencing factors of the TVMS in MEs and AEs. Both profile modification and lead crowning reduced the mean of the TVMS. The proposed method is expected to provide accurate TVMS excitation data of gear transmission systems for dynamic analysis.

C. Liu · W. Shi (✉) · K. Liu
State Key Laboratory of Mechanical Transmission, Chongqing University, Chongqing 400044, People's Republic of China
e-mail: shi_wankai@sina.com

C. Liu
e-mail: chang_liu@cqu.edu.cn

K. Liu
e-mail: kun_liu@cqu.edu.cn

List of symbols

a	Standard center distance between two gears
A_x	Area of section
B, B^i	Width of tooth and slice
C_a, C_b	Maximum modification amounts of profile modification and lead crowning
C_F	Correction factor considering coupling effect between adjacent slices
dx	Coefficient defined in Fig. 7
$D_g^{\Delta Z}$	Minimum distance from arc $\Gamma_g^{\Delta Z}$ center to arc $\Gamma_p^{\Delta Z}$
$D_p^{\Delta Z}$	Minimum distance from arc $\Gamma_p^{\Delta Z}$ center to arc $\Gamma_g^{\Delta Z}$
$D_{gp}^{\Delta Z}$	Minimum distance between arc $\Gamma_g^{\Delta Z}$ and $\Gamma_p^{\Delta Z}$
e	Calculation accuracy
e_c	Coefficient of modification curve
e_g^i, e_p^i	Initial gaps between axial slices
E	Young's modulus

E_{sni}, E_{sns}	Lower and upper deviations of tooth thickness
f_{pt}	Single pitch deviation
F_p	Total cumulative pitch deviation
F_α	Total profile deviation
F_β	Helix deviation
G	Shear modulus
h, h_x	Coefficients defined in Fig. 7
i	Index of discrete elements along tooth width
i_c	Index of contacted tooth pairs
i_g, i_p	Index of slices where Hertzian contact center is located on gear and pinion
I_x	Area moment of inertia
j	Index of discrete elements along tooth profile
k_a^{ij}	Axial compressive stiffness
k_b^{ij}	Bending stiffness
k_f^{ij}	Stiffness considering gear fillet-foundation deflection
k_f^*, k_f^{i*}	Correction foundation stiffnesses of gear and slice
$k_{h\_ic}^t$	Hertzian contact stiffness
k_{mesh}	Time-varying mesh stiffness
k_s^{ij}	Shear stiffness
k_{tooth_p,g_ic}^t	Tooth stiffness of nominal slice $S_{N\_ic}^t$ on tooth pair i_c
L	Coefficient defined in Fig. 7
L_1, L_2	Profile modification length and half of lead crowning length
L^*, M^*, P^*, Q^*	Coefficients in Eq. (27)
n	Index of teeth
n_1, n_2	Number of discrete elements along tooth width and profile
n_3	Number of contact tooth pairs
n_4	Number of nominal slices on contact tooth pair i_c
n_{lg}, n_{lp}	Half of number of uncontacted slices between current and last contact slices on gear and pinion
n_{ng}, n_{np}	Half of number of uncontacted slices between current and next contact slices on gear and pinion

R	Reference radius
r_b	Radius of base circle
$r_g^{\Delta Z}, r_p^{\Delta Z}$	Radii of arcs $\Gamma_g^{\Delta Z}$ and $\Gamma_p^{\Delta Z}$
r_L^{nij}, r_R^{nij}	Radii of circles where control points of elements Σ_L^{nij} and Σ_R^{nij} are located
$R_{pt}(1), R_{Es}(1), R_\alpha(1),$ $R_\beta(1)$	Variables with a value range of [0, 1] and obey different probability distributions
S_1, S_2	Modification distances of profile modification and lead crowning
S_f	Coefficient defined in Fig. 7
S^i, S_g^i, S_p^i	Axial slices
S_N^t	Nominal slice
t	Index of contacted nominal slices
T_g	Output torque of gear
u_f	Coefficient defined in Fig. 7
W_F^i	Weighting factor of the slice S^i
W_k	Base tangent length
x	Coefficient defined in Fig. 7
z	Number of teeth
$X_c^{ij}, Y_c^{ij}, Z_c^{ij}$	Coordinates of center of curvature corresponding to control point of discrete element
$X_L^{1ij}, Y_L^{1ij}, Z_L^{1ij}, X_R^{1ij},$ Y_R^{1ij}, Z_R^{1ij}	Theoretical coordinates of element control point on surfaces of first tooth
$X_{MEL}^{nij}, Y_{MEL}^{nij}, Z_{MEL}^{nij},$ $X_{MER}^{nij}, Y_{MER}^{nij}, Z_{MER}^{nij}$	Coordinates of element control point considering manufacturing errors (MEs)
$X_{TML}^{nij}, Y_{TML}^{nij}, Z_{TML}^{nij},$ $X_{TMR}^{nij}, Y_{TMR}^{nij}, Z_{TMR}^{nij}$	Coordinates of element control point considering MEs and tooth modifications (TMs)
$X_{AEL}^{nij}, Y_{AEL}^{nij}, Z_{AEL}^{nij},$ $X_{AER}^{nij}, Y_{AER}^{nij}, Z_{AER}^{nij}$	Coordinates of element control point considering MEs, TMs, and assembly errors (AEs)

Greek symbols

β	Helix angle of reference circle
β_j	Coefficient defined in Fig. 7
δ_f, δ_g	Foundation deflections

$\delta_{N\_i_c}^{t}$	Comprehensive deflection of nominal slice
$\delta_{i_c}^{t}$	Total deflection of contact center of nominal slice
Δ_1, Δ_2	Modification amounts of profile modification and lead crowning
Δ_{sum}	Total amount of TMs
$\Delta x, \Delta y$	Center distance deviations along X-axis and Y-axis
ΔZ	Distance between centers of arc $\Gamma^{\Delta Z}$ and arc corresponding to element control point
$\Delta\theta_1, \Delta\theta_2$	Rotation steps of gear and pinion
$\Delta\theta_c$	Angle parameter used for calculating center coordinates of arc $\Gamma^{\Delta Z}$
$\Delta\theta_{MEL}^{nij}, \Delta\theta_{MER}^{nij}$	Angle parameters used for generating tooth surfaces with MEs in Eqs. (5) and (6)
$\Delta\theta_{TML}^{nij}, \Delta\theta_{TMR}^{nij}$	Angle parameters used to generate tooth surfaces with TMs in Eqs. (12) and (13)
$\Sigma_L^{nij}, \Sigma_R^{nij}$	Discrete elements on tooth surfaces
$\Sigma^{\Delta Z}$	Plane perpendicular to Z-axis
$\Gamma^{\Delta Z}$	Arc on discrete element
υ	Poisson's ratio
θ_1, θ_2	Rotation angles of gear and pinion during iterative process for calculating time-varying mesh stiffness (TVMS)
θ_f	Coefficient defined in Fig. 7
φ, γ	Misalignment deviations on XB_pZ-plane and YB_pZ-plane
η, λ	Correction coefficients of foundation stiffness

Acronyms

AEs	Assembly errors
FEM	Finite element method
MEs	Manufacturing errors
TCA	Tooth contact analysis
TMs	Tooth modifications
TVMS	Time-varying mesh stiffness

1 Introduction

Gear transmissions are widely used in various types of mechanical equipment, such as automobiles, helicopters, and shearers, to transmit power and motion. As the popularity of electric vehicles grows, the requirements on the noise, vibration, and harshness (NVH) performances of automobile are becoming increasingly stringent, which has become a subject of great relevance in recent years. The sources of vibration and noise of gear transmission systems are commonly divided into internal and external excitations, and the time-varying mesh stiffness (TVMS) is one of the most important internal excitations [1]. Therefore, the accurate calculation of the TVMS is of great significance for the analysis and control of the vibrations and noise of gear transmission systems.

In previous studies, analytical methods and the finite element method (FEM) were the two most important methods for calculating the TVMS [2]. The FEM has been generally accepted and is widely used due to its accuracy and its ability to calculate the stiffnesses of arbitrary bodies with complex shapes [3]. For example, Wang and Howard [4] and Yuan et al. [5] investigated the effects of different loads on the TVMS of spur and helical gear pairs, respectively. Ma et al. [6] investigated the influence of different amounts of profile modification on the TVMS of spur gear pairs. Shao et al. [7] investigated the effects of gear faults on the TVMS of spur gear pairs and obtained the relationship between the TVMS and the gear vibrations. Cooley et al. [8] compared the differences between the local slope method and the average slope method in calculating the TVMS by the FEM. In addition, the FEM is often used to verify the accuracy of analytical methods [9, 10]. With the development of computing technology in recent years, although the FEM has been used in various fields, there are still many problems in the calculation of the TVMS. On the one hand, the calculation accuracy of the FEM depends on the mesh quality, which is related to the mesh size. In general, the mesh size is difficult to approximate at the micrometer level, which is the size range of manufacturing errors (MEs), to ensure the calculation efficiency and cost. On the other hand, the MEs of each tooth, such as pitch deviations, are different in practice, and different tooth meshing sequences also affect the calculation results of the TVMS. However, to avoid very large finite element models, usually only some of the teeth of the gear pair are considered in the model. Therefore, the FEM is not an effective method to calculate the TVMS when MEs are considered.

Compared with the FEM, analytical methods have higher computational efficiencies, and their results are

in good agreement with the FEM. As a result, analytical methods have received considerable attention in recent years, and many analytical models have been proposed in the literature. Cornell [11] and Weber [12] calculated the stiffnesses of spur gear teeth using materials mechanics approaches, and these methods were extended by Sainsot et al. [13] and Chen et al. [14]. Yang and Lin [15] presented the potential energy method for calculating the TVMS. This method was further developed by Tian [16] and Wu et al. [17] considering the influence of shear deflection. This method was extended and is widely used in the study of the TVMS. For example, Chaari et al. [18] and Wan et al. [19] studied the effect of tooth cracking on the TVMS of spur gear pairs. Chen and Shao [20] studied the effects of gear tooth errors, tooth profile modifications, applied loads, and tooth root cracks on the TVMS of spur gear pairs. Chen et al. [1] revealed the influence mechanisms of the coupling effect of the gear body structure on the TVMS of spur gear pairs. The TVMS was also approximated by rectangular waves in some studies [21–23].

The aforementioned analytical methods focus more on the TVMS calculation of spur gear pairs. The TVMS analytical methods of helical gear pairs mainly focus on the comprehensive application of the slice method and the potential energy method, in which the helical gear is divided into multiple spur gear slices along the tooth width. For example, Wang and Zhang [24] established a TVMS model of a helical gear pair considering the influence of tooth profile errors. Wan et al. [25] presented the accumulated integral potential energy method for calculating the TVMS of normal and faulty helical gears. Jiang and Liu [26] and Huangfu et al. [10] proposed other efficient TVMS analytical methods for helical gear pairs to analyze the influence of tooth cracks. Han et al. [27] developed a TVMS model of a helical gear pair considering the effect of friction. Feng et al. [28] proposed an improved analytical method taking the influence of the effective elastic modulus, the nonlinear Hertzian contact, and various coefficients, such as the modification, friction, and fillet-foundation coefficients, into consideration. Yu and Mechefske [9] also presented an improved analytical method considering the coupling influence between adjacent slices. Marques et al. [29] established a TVMS analytical model based on the tooth stiffness in a unit length of a single contact line and the maximum tooth stiffness in the ISO 6336

standard. Although many analytical methods have been proposed in the past and these methods have higher efficiencies than the FEM, there is no prediction method for the TVMS based on the gear accuracy grade, as only the tolerance ranges of MEs are usually defined in the gear design stage.

In addition, a reasonable loaded tooth contact analysis algorithm is the key to accurately calculating the TVMS in an analytical method. The generalized tooth contact analysis algorithm suffers from a complicated calculation process and numerical instability [30]. Moreover, when the influence of the tooth errors is considered, the actual meshing position is difficult to determine through the traditional tooth contact analysis algorithm [31]. It is usually assumed that the actual position is still on the theoretical meshing line, and the tooth error is regarded as a displacement parameter along the theoretical line of action [1, 31, 32]. However, owing to the effects of tooth errors, not only has the actual meshing position changed, but also some special meshing phenomena will occur during the transmission process, such as the loss of contact of tooth pairs, out-of-line meshing, and eccentric loads. Although all major commercial non-FE gear analysis tools are able to calculate the TVMS of gear pairs, most of them are based on the ISO standard, and the influence of the above abnormal meshing phenomena on the TVMS is also not considered.

This study presents a novel analytical method for calculating the TVMS of helical gear pairs considering the effects of MEs, AEs, and TMs. The first section reviews the calculation methods of the TVMS. A novel calculation method of the TVMS is proposed in Sect. 2. The presented method is verified by comparing the results with the literature in Sect. 3. Section 4 shows a series of TVMS results obtained by the novel calculation method, and the influence mechanisms of MEs, AEs, and TMs on the TVMS are discussed. Finally, Sect. 5 presents the conclusions of this study, and the significance of the proposed method is summarized.

2 Principles of novel calculation method

MEs, AEs, and TMs are inevitable in the practical application of gears, which will change the tooth contact, such as causing early or delayed contact. A

reasonable generation method of the actual error of the tooth surface and the development of a tooth contact analysis (TCA) algorithm on this basis are the keys to accurately calculating the TVMS of helical gear pairs. Therefore, Sect. 2.1 first establishes a practical gear error model considering MEs, AEs, and TMs. A novel TCA algorithm based on the proposed gear model is developed in Sect. 2.2. Finally, the calculation process of the TVMS is described in Sect. 2.3.

2.1 Gear model

In most of the existing calculation methods, the effects of MEs are not considered, and the gears are regarded as perfect tooth surfaces without errors. In some studies, specific assumptions were made about the MEs of gears. For example, Kurokawa et al. [33] assumed that the MEs of each tooth were the same, and the accumulative pitch error was also assumed to be distributed as a sine wave in other studies [5, 34, 35]. However, usually only the gear accuracy grades, that is, the tolerance ranges of the MEs, are determined in the gear design process. Moreover, the MEs of each tooth are different in practice, and the TVMS is also affected by the different tooth meshing sequences. The gear models in the existing methods cannot represent gears with MEs directly and effectively. In this section, a practical gear error model based on the gear accuracy grade is proposed, in which MEs (single pitch deviation, total cumulative pitch deviation, total profile deviation, total helix deviation, tooth thickness deviation, and base tangent length), AEs (center distance and misalignment deviations), and TMs (profile modification and lead crowning) are considered.

In this study, the tooth surfaces are discretized into $n_1 \times n_2$ elements of the same size, as shown in Fig. 1a. The control point of each element is located at its center and is denoted by the indices i and j. It is known that different types of MEs are distributed according to a probability within their tolerance ranges, which can be found in the ISO standard [36] of the gear accuracy grade. To generate the actual tooth surfaces considering MEs, first, the theoretical coordinates of the element control points on the surfaces of the first tooth, $\left(X_{\mathrm{L}}^{1ij}, Y_{\mathrm{L}}^{1ij}, Z_{\mathrm{L}}^{1ij}\right)$, and $\left(X_{\mathrm{R}}^{1ij}, Y_{\mathrm{R}}^{1ij}, Z_{\mathrm{R}}^{1ij}\right)$, are obtained by the standard involute

equation, where the subscripts L and R indicate that the element control point is located on the left and right tooth surface, respectively. The tooth surfaces on both sides of each tooth will be generated based on the different MEs in sequence. The MEs of the control points on the nth tooth surface are given as follows:

$$f_{\mathrm{pt}}^n = \left(-f_{\mathrm{pt}}\right) + R_{\mathrm{pt}}(1)\left(2f_{\mathrm{pt}}\right), \tag{1}$$

$$E_{\mathrm{s}}^n = E_{\mathrm{sni}} + R_{\mathrm{Es}}(1)\left(E_{\mathrm{sns}} - E_{\mathrm{sni}}\right), \tag{2}$$

$$F_{\alpha}^{nij} = \left(R_{\alpha}(1) - 1/2\right)F_{\alpha}, \tag{3}$$

$$F_{\beta}^{ni} = \left(R_{\beta}(1) - 1/2\right)F_{\beta}, \tag{4}$$

where $R_{\mathrm{pt}}(1)$, $R_{\mathrm{Es}}(1)$, $R_{\alpha}(1)$, and $R_{\beta}(1)$ are variables with a value range of [0, 1] and obey different probability distributions; f_{pt}, F_{α}, and F_{β} are the tolerance ranges of the single pitch deviation, total profile deviation, and helix deviation, respectively; E_{sni} and E_{sns} are the lower and upper deviations of the tooth thickness, respectively; and the superscripts n, i, and j identify the control point of element $i \times j$ on the nth tooth.

The tooth surfaces with MEs of the nth tooth are given as follows:

$$\begin{bmatrix} X_{\mathrm{MEL}}^{nij} \\ Y_{\mathrm{MEL}}^{nij} \\ Z_{\mathrm{MEL}}^{nij} \end{bmatrix} = \begin{bmatrix} \cos\left(\Delta\theta_{\mathrm{MEL}}^{nij}\right) & \sin\left(\Delta\theta_{\mathrm{MEL}}^{nij}\right) & 0 \\ -\sin\left(\Delta\theta_{\mathrm{MEL}}^{nij}\right) & \cos\left(\Delta\theta_{\mathrm{MEL}}^{nij}\right) & 0 \\ 0 & 0 & 1 \end{bmatrix} \begin{bmatrix} X_{\mathrm{L}}^{1ij} \\ Y_{\mathrm{L}}^{1ij} \\ Z_{\mathrm{L}}^{1ij} \end{bmatrix}, \tag{5}$$

$$\begin{bmatrix} X_{\mathrm{MER}}^{nij} \\ Y_{\mathrm{MER}}^{nij} \\ Z_{\mathrm{MER}}^{nij} \end{bmatrix} = \begin{bmatrix} \cos\left(\Delta\theta_{\mathrm{MER}}^{nij}\right) & \sin\left(\Delta\theta_{\mathrm{MER}}^{nij}\right) & 0 \\ -\sin\left(\Delta\theta_{\mathrm{MER}}^{nij}\right) & \cos\left(\Delta\theta_{\mathrm{MER}}^{nij}\right) & 0 \\ 0 & 0 & 1 \end{bmatrix} \begin{bmatrix} X_{\mathrm{R}}^{1ij} \\ Y_{\mathrm{R}}^{1ij} \\ Z_{\mathrm{R}}^{1ij} \end{bmatrix}. \tag{6}$$

The angle parameters, $\Delta\theta_{\mathrm{MEL}}^{nij}$ and $\Delta\theta_{\mathrm{MER}}^{nij}$, can be calculated as follows:

$$\Delta\theta_{\mathrm{MEL}}^{nij} = [2\pi(n-1)]/z + \left(\sum_{z=1}^n f_{\mathrm{pt}}^n + F_{\alpha L}^{nij}\right)\bigg/ r$$
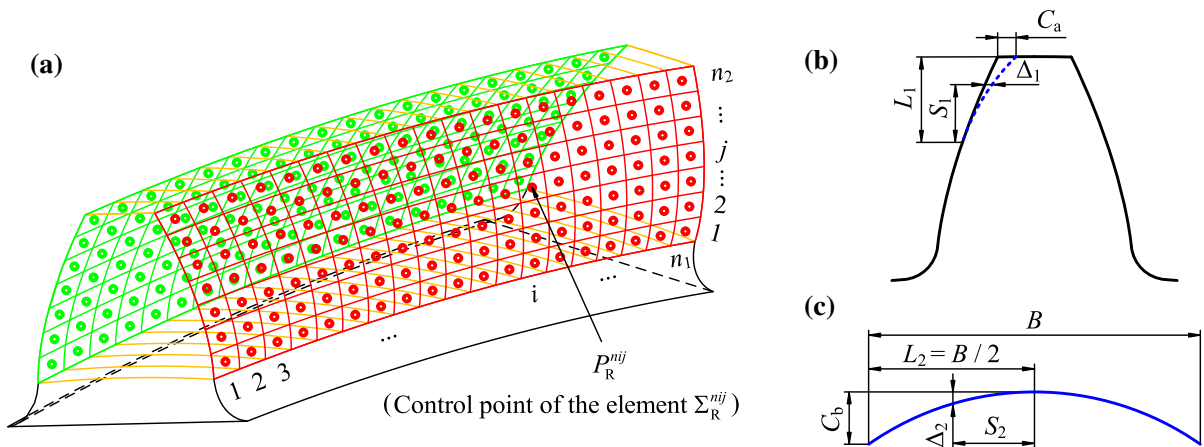$$+ F_{\beta L}^{ni}\bigg/(r_{\mathrm{b}}\cos\beta), \tag{7}$$

Fig. 1 **a** Discrete tooth surfaces of helical gear, **b** profile modification, and **c** lead crowning

$$\Delta\theta_{\text{MER}}^{nij} = [2\pi(n-1)]/z + \left(\sum_{z=1}^{n} f_{\text{pt}}^{n} + E_{\text{s}}^{n} + F_{\alpha R}^{nij}\right) \Big/ r$$
$$+ F_{\beta R}^{ni} \Big/ (r_{\text{b}}\cos\beta), \tag{8}$$

where β is the helix angle of the reference circle, and z is the number of teeth, and r and r_{b} are the reference radius and the radius of the base circle, respectively. It is worth noting that after each tooth surface is generated based on Eqs. (5) and (6), the total cumulative pitch deviation (F_{p}) and the base tangent length (W_{k}) will be used to check that the values of f_{pt}^{n}, E_{s}^{n}, F_{α}^{nij}, and F_{β}^{ni} are reasonable. If F_{p} and W_{k} are not within their tolerance ranges, f_{pt}^{n}, E_{s}^{n}, F_{α}^{nij}, and F_{β}^{ni} will be reassigned.

After tooth surfaces with MEs are generated, TMs are introduced into the gear model, where the profile modification and the lead crowning are considered (see Fig. 1b, c). Both TMs are obtained by moving the control points of each element. It is assumed that the maximum modification amounts of the profile modification and the lead crowning are C_{a} and C_{b}, respectively. B is the tooth width, L_1 is the length of the profile modification, and L_2 is half the lead crowning length. When the modification distance is S_1, the amount of profile modification is given as follows:

$$\Delta_1 = C_{\text{a}}(S_1/L_1)^{e_{\text{c}}}, \tag{9}$$

where e_{c} is the coefficient of the modification curve. If the modification curve is a straight line, $e_{\text{c}} = 1$. If the modification curve is a parabola, $e_{\text{c}} = 2$.

Similarly, when the modification distance is S_2, the amount of the lead crowning is given as follows:

$$\Delta_2 = C_{\text{b}}(S_2/L_2)^2. \tag{10}$$

For each element on the tooth surface, the total TM amount can be calculated as follows:

$$\Delta_{\text{sum}} = \Delta_1 + \Delta_2. \tag{11}$$

The tooth surfaces with MEs and TMs of the nth tooth are given as follows:

$$\begin{bmatrix} X_{\text{TML}}^{nij} \\ Y_{\text{TML}}^{nij} \\ Z_{\text{TML}}^{nij} \end{bmatrix} = \begin{bmatrix} \cos(\Delta\theta_{\text{TML}}^{nij}) & -\sin(\Delta\theta_{\text{TML}}^{nij}) & 0 \\ \sin(\Delta\theta_{\text{TML}}^{nij}) & \cos(\Delta\theta_{\text{TML}}^{nij}) & 0 \\ 0 & 0 & 1 \end{bmatrix} \begin{bmatrix} X_{\text{MEL}}^{nij} \\ Y_{\text{MEL}}^{nij} \\ Z_{\text{MEL}}^{nij} \end{bmatrix}, \tag{12}$$

$$\begin{bmatrix} X_{\text{TMR}}^{nij} \\ Y_{\text{TMR}}^{nij} \\ Z_{\text{TMR}}^{nij} \end{bmatrix} = \begin{bmatrix} \cos(\Delta\theta_{\text{TMR}}^{nij}) & -\sin(\Delta\theta_{\text{TMR}}^{nij}) & 0 \\ \sin(\Delta\theta_{\text{TMR}}^{nij}) & \cos(\Delta\theta_{\text{TMR}}^{nij}) & 0 \\ 0 & 0 & 1 \end{bmatrix} \begin{bmatrix} X_{\text{MER}}^{nij} \\ Y_{\text{MER}}^{nij} \\ Z_{\text{MER}}^{nij} \end{bmatrix}, \tag{13}$$

where $\Delta\theta_{\text{TML}}^{nij} = -\left(\Delta_{\text{sumL}}^{nij}/r_{\text{L}}^{nij}\right)$, and $\Delta\theta_{\text{TMR}}^{nij} = \Delta_{\text{sumR}}^{nij}/r_{\text{R}}^{nij}$. $\Delta_{\text{sumL}}^{nij}$ and $\Delta_{\text{sumR}}^{nij}$ are the total TM amounts of the elements Σ_{L}^{nij} and Σ_{R}^{nij}, respectively. Similarly, r_{L}^{nij} and r_{R}^{nij} are the radii of the circles where the control points of the elements Σ_{L}^{nij} and Σ_{R}^{nij} are located, respectively.

The part of the tooth surface with MEs and TMs is shown in Fig. 2a. Unlike the gear model in traditional analytical methods, the tooth surfaces with errors are
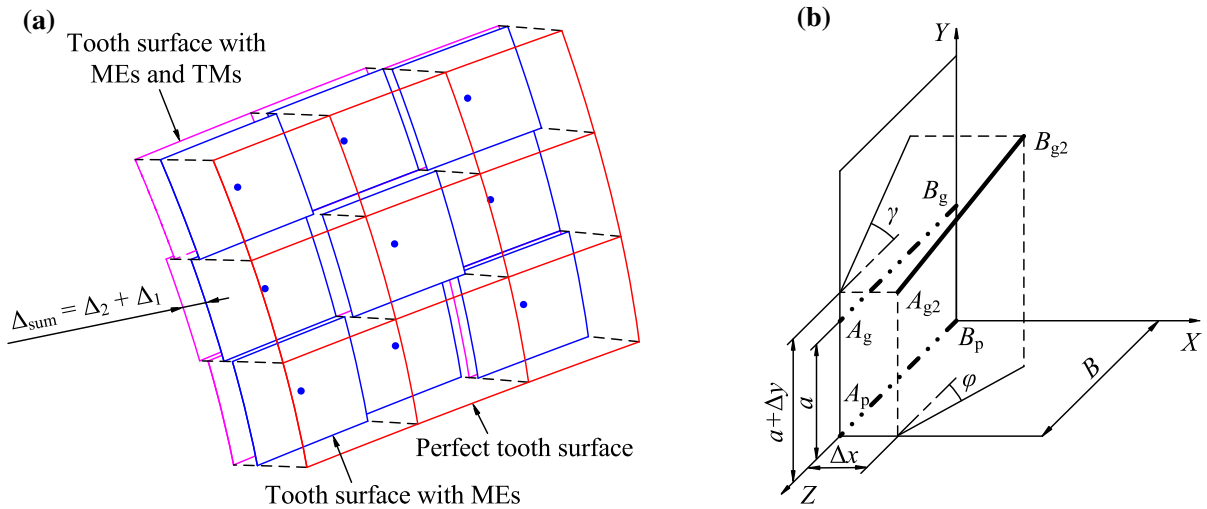
Fig. 2 **a** Part of the tooth surface with MEs and TMs and **b** definition of AEs

not smooth and consist of multiple elements of the same size. Figure 2b shows the definition of the AEs used in this study. A_gB_g and A_pB_p are the theoretical axis positions of the gear and pinion without AEs, respectively. The AEs of the gear and pinion are equivalently transferred to the axis position of the gear to simplify the model in this study. $A_{g2}B_{g2}$ is the new axis position of the gear when the AEs are considered. The AEs are indicated by four parameters, where Δx and Δy are called the center distance deviations, φ and γ are the misalignment deviations on the XB_pZ-plane and YB_pZ-plane, respectively, and a is the standard center distance. The different AEs can be obtained by different combinations of the above four parameters. Therefore, the surfaces with MEs, TMs, and AEs of the nth tooth are given as follows:

$$\begin{bmatrix} X_{\text{AEL}}^{nij} \\ Y_{\text{AEL}}^{nij} \\ Z_{\text{AEL}}^{nij} \\ 1 \end{bmatrix} = \begin{bmatrix} 1 & 0 & M_{13} & M_{14} \\ 0 & 1 & M_{23} & M_{24} \\ 0 & 0 & M_{33} & M_{34} \\ 0 & 0 & 0 & 1 \end{bmatrix} \begin{bmatrix} X_{\text{TML}}^{nij} \\ Y_{\text{TML}}^{nij} \\ Z_{\text{TML}}^{nij} \\ 1 \end{bmatrix}, \quad (14)$$

$$\begin{bmatrix} X_{\text{AER}}^{nij} \\ Y_{\text{AER}}^{nij} \\ Z_{\text{AER}}^{nij} \\ 1 \end{bmatrix} = \begin{bmatrix} 1 & 0 & M_{13} & M_{14} \\ 0 & 1 & M_{23} & M_{24} \\ 0 & 0 & M_{33} & M_{34} \\ 0 & 0 & 0 & 1 \end{bmatrix} \begin{bmatrix} X_{\text{TMR}}^{nij} \\ Y_{\text{TMR}}^{nij} \\ Z_{\text{TMR}}^{nij} \\ 1 \end{bmatrix}, \quad (15)$$

where $M_{13} = (1 - \sin\gamma)\tan\varphi - \sin\varphi$, $M_{23-} = -\sin\gamma/\cos\varphi$, $M_{33} = \sin\gamma - \cos\varphi - 1$, $M_{14-} = \Delta x + B[\sin\varphi - (1 - \sin\gamma)\tan\varphi]$, $M_{24-} = a + \Delta y + B_c\sin\gamma/\cos\varphi$, $M_{34} = B(\cos\varphi + 1 - \sin\gamma)$.

2.2 Novel tooth contact analysis (TCA) algorithm based on proposed gear model

Because of the effects of MEs, AEs, and TMs, some special contact situations will occur during the meshing process, such as the contact points being outside the theoretical meshing line and discontinuous on the tooth surface. In order to accurately determine the position of the actual contact point on the tooth surfaces and calculate the amount of deflection at different meshing positions of the gear pair, a novel TCA algorithm based on the presented gear model is developed in this section, in which the tooth contact is converted into the contact of discrete elements on the tooth surface. In Sect. 2.1, the coordinates of the control point of each element and their corresponding radius of curvature have been calculated, based on which the center of curvature corresponding to each control point can also be obtained. Since the tooth surface of a helical gear can be regarded as generated by the translation and rotation of the transverse profile around the gear axis, each element on the tooth surface is represented as a helical surface consisting of a series of arcs in this algorithm, as shown in Fig. 3a. The radii
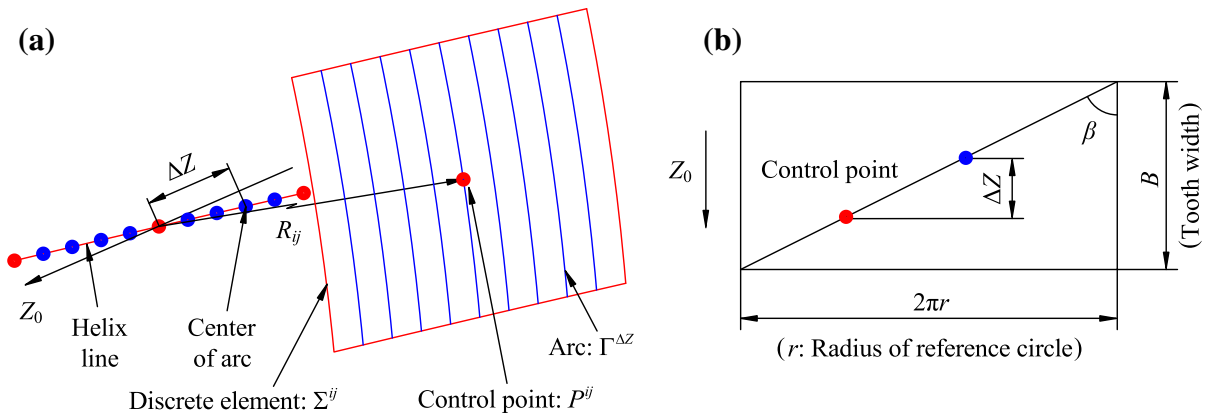
Fig. 3 Tooth surface: **a** helical arc surface used to represent discrete element and **b** development drawings of the tooth surface

of these arcs are the same as the radius of curvature at the control point, and their centers are located on a helix line. Hence, determining the coordinates of these arc centers is the key to representing the helical arc surface of each element by mathematical equations.

In Fig. 3a, the Z_0-axis is the axis of the helical arc surface, which is parallel to the gear axis. The arc $\Gamma^{\Delta Z}$ is the intersection line of the element Σ^{ij} and the plane perpendicular to the Z_0-axis. The distance between the center of the arc $\Gamma^{\Delta Z}$ and the center of curvature corresponding to the control point along the Z_0-axis is denoted as ΔZ. The arc center coordinates can be obtained by the translation and rotation of the coordinates of the center of curvature $\left(X_c^{ij}, Y_c^{ij}, Z_c^{ij}\right)$ corresponding to the control point around the Z_0-axis. Therefore, the center coordinates of the arc $\Gamma^{\Delta Z}$ are given as follows:

$$
\begin{bmatrix} X_{\Delta Z}^{ij} \\ Y_{\Delta Z}^{ij} \\ Z_{\Delta Z}^{ij} \end{bmatrix} = \begin{bmatrix} \cos(\Delta\theta_c) & -\sin(\Delta\theta_c) & 0 \\ \sin(\Delta\theta_c) & \cos(\Delta\theta_c) & 0 \\ 0 & 0 & 1 \end{bmatrix} \begin{bmatrix} X_c^{ij} \\ Y_c^{ij} \\ Z_c^{ij} - \Delta Z \end{bmatrix},
$$

(16)

where $\Delta\theta_c$ is the rotation angle around the Z_0-axis. According to the development drawings of the tooth surface (see Fig. 3b), the rotation angle can be calculated as follows:

$$
\Delta\theta_c = \frac{\Delta Z \tan\beta}{r}.
$$

(17)

For an arbitrary output position, the gear is fixed, and the pinion is rotated counterclockwise to approach the gear. During the rotation process of the pinion,

there are four cases for two arbitrary elements (Σ_g^{ij} and Σ_p^{ij}) with common x, y, and z ranges on the tooth surfaces of the two gears, as shown in Fig. 4. When the AEs are not considered, the axes of Σ_g^{ij} and Σ_p^{ij} are parallel to the Z-axis (see Fig. 4a, b). In an arbitrary plane perpendicular to the Z-axis ($\Sigma^{\Delta Z}$), Σ_g^{ij} and Σ_p^{ij} can be represented as the arcs $\Gamma_g^{\Delta Z}$ and $\Gamma_p^{\Delta Z}$, respectively. The minimum distance between the two arcs ($D_{gp}^{\Delta Z}$) is used to determine whether the two elements are in contact, which can be calculated as follows:

$$
D_{gp}^{\Delta Z} = \frac{\left(r_g^{\Delta Z} - D_g^{\Delta Z}\right) + \left(r_p^{\Delta Z} - D_p^{\Delta Z}\right)}{2},
$$

(18)

where $r_g^{\Delta Z}$ and $r_p^{\Delta Z}$ are the radii of the arcs $\Gamma_g^{\Delta Z}$ and $\Gamma_p^{\Delta Z}$, respectively, and $D_g^{\Delta Z}$ is the minimum distance between the $\Gamma_g^{\Delta Z}$ arc center and each point on the arc $\Gamma_p^{\Delta Z}$. Similarly, $D_p^{\Delta Z}$ is the minimum distance between the arc $\Gamma_p^{\Delta Z}$ center and each point on the arc $\Gamma_g^{\Delta Z}$. If $D_{gp}^{\Delta Z}$ is less than zero, the elements Σ_g^{ij} and Σ_p^{ij} are separate, as shown in Fig. 4a. Otherwise, they are in contact, as shown in Fig. 4b. Similarly, when the AEs are considered, the judgement of whether the two elements are in contact is performed in the same way. It is worth noting that the axis of Σ_g^{ij} is not parallel to the Z-axis because the AEs are equivalently transferred to the gear axis. Therefore, $D_{gp}^{\Delta Z}$ is not the minimum distance between the two arcs ($\Gamma_g^{\Delta Z}$ and $\Gamma_p^{\Delta Z}$), it is the minimum distance between the arc $\Gamma_p^{\Delta Z}$ and the projection of the arc $\Gamma_g^{\Delta Z}$ on the plane $\Sigma^{\Delta Z}$ (see
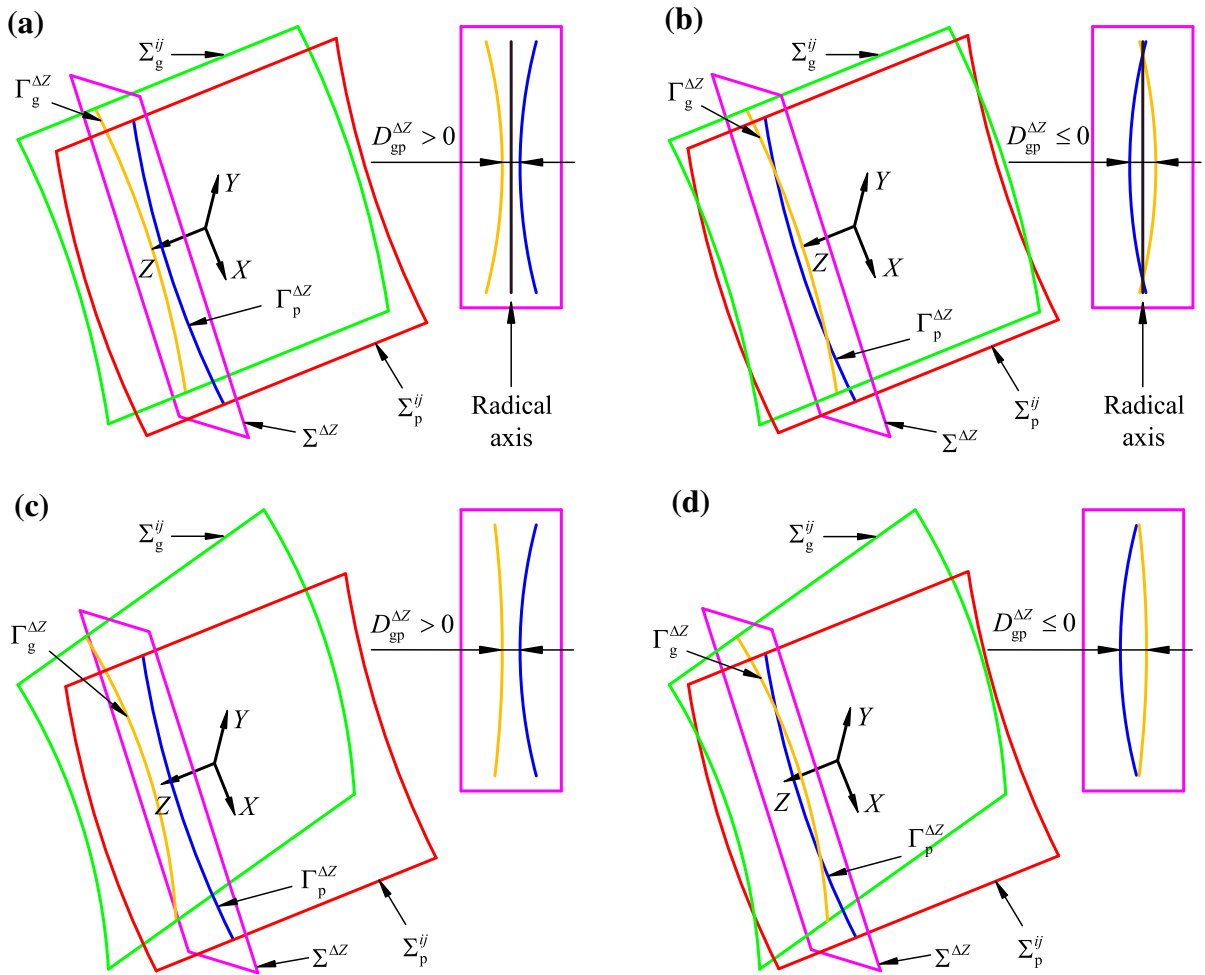
Fig. 4 Four cases of two arbitrary elements with common x, y, and z ranges on two gears: **a** element separation without AEs, **b** element contact without AEs, **c** element separation with AEs, and **d** element contact with AEs

Fig. 4c, d). In addition, under load conditions, the pinion will continue to rotate after the two gears make contact until the output torque of the gear balances the external load. The mean of all the minimum distances ($D_{gp}^{\Delta Z}$) corresponding to different planes perpendicular to the Z-axis ($\Sigma^{\Delta Z}$) is defined as the total deflection of the two elements.

2.3 Time-varying mesh stiffness calculation

The slice method has been widely used in the study of the TVMS of helical gear pairs [9, 10, 24–28], in which the helical gear is usually divided into multiple slices along the axial direction. In this study, the discrete tooth surfaces of the helical gear are regarded as consisting of n_1 slices, each of which consists of n_2 elements (see Fig. 1a). The TVMS of the helical gear pair is calculated through an iterative process in this study (see Fig. 5). First, the gear model with tooth surfaces containing errors is generated based on the input gear data, MEs, AEs, and TMs. It can also be generated using the measurement coordinates of the control point of each discrete element. The first positions of the gear (θ_1) and the pinion (θ_2) are initialized to zero. In addition, the calculation accuracy (e) and the rotation step sizes of the gear ($\Delta\theta_1$) and the pinion ($\Delta\theta_2$) are also defined. Second, the gear is rotated clockwise by $\Delta\theta_1$ to an output position and then fixed, and the pinion is rotated counterclockwise by a smaller step ($\Delta\theta_2$) to approach the gear. After each rotation of the pinion, the contact status between
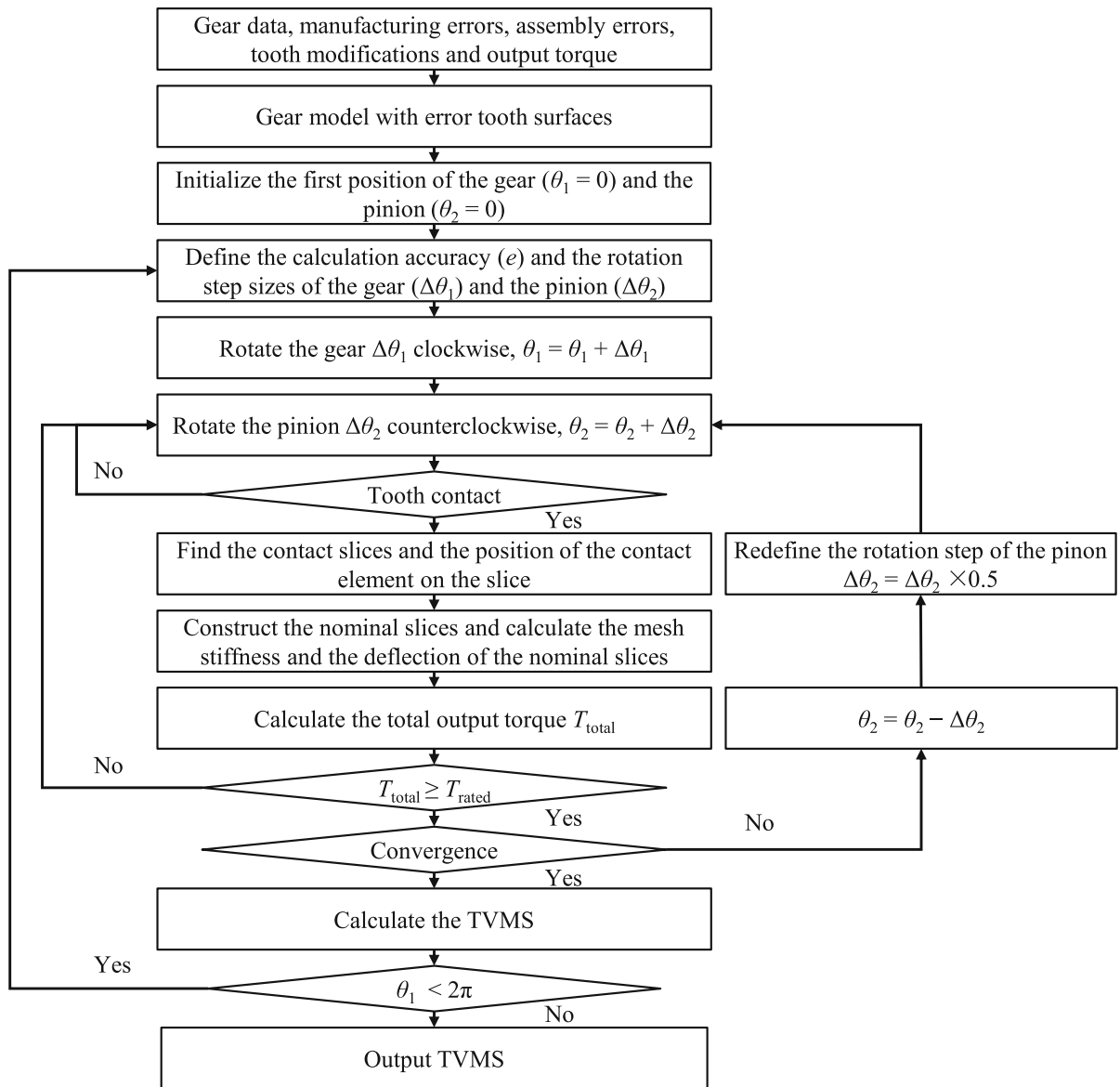
Fig. 5 Flowchart of the calculation of the TVMS

the gear and pinion is checked based on the proposed TCA algorithm.

When the effects of MEs, AEs, and TMs are not considered, that is, when the tooth surfaces are perfect, the contact center of each slice is located on the theoretical contact line (see the blue line in Fig. 6a). However, when the effects of MEs, AEs, and TMs are considered, there are different initial gaps (e_g^i and e_p^i) between the axial slices (S_g^i and S_p^i) on the two gears (see Fig. 6b). As the pinion rotates counterclockwise,

these gaps will decrease until the resultant force of all the contact slices is balanced with the external load. Due to the effects of the MEs, AEs, and TMs, it is inevitable that parts of the slices will lose contact (see Fig. 6c) or the contact center on a slice will lie outside the theoretical contact line. The yellow line segment in Fig. 6a shows an actual possible contact line. In a previous report [24], each slice along the tooth width was independent, which meant the deflection on one slice could not be conveyed to the neighboring slices. This method will introduce large errors to the
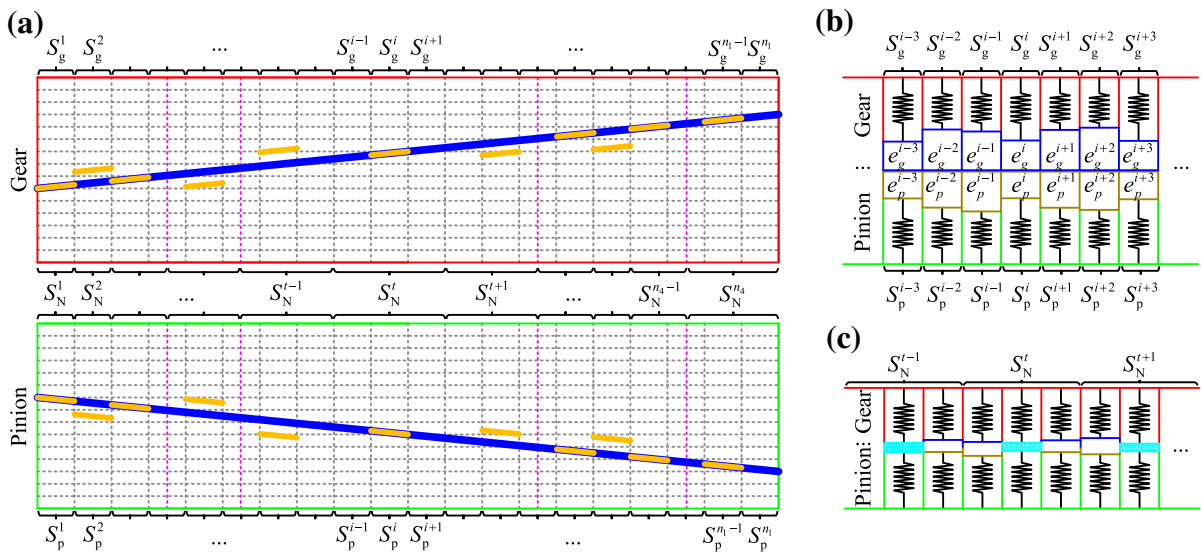
Fig. 6 Tooth contact of helical gear pair: **a** definition of nominal slice, **b** initial gaps between axial slices, and **c** contact of nominal slice

calculation results of the TVMS when parts of the slices lose contact. Hence, the definition of the nominal slice is proposed in this study, as shown in Fig. 6a. It is assumed that there are n_3 contact tooth pairs, and each tooth pair includes n_4 nominal slices (the value of n_4 may not be equal for different contact tooth pairs). For each contact tooth pair, the construction law of the nominal slice is given as follows:

1. A nominal slice consists of a contact slice and non-contact slices on both sides, and the number of non-contact slices on both sides participating in the construction of the nominal slice is half of the total number of non-contact slices on both sides (see Fig. 6a, nominal slice S_N^t).

2. If the adjacent slices on both sides of a contact slice are also contact slices, only the contact slice constitutes a nominal slice (see Fig. 6a, nominal slices S_N^1 and S_N^2).

3. If the number of non-contact slices between two adjacent contact slices is an odd number, the central slice is subdivided into two identical slices so that the number of non-contact slices is an even number (see Fig. 6a, nominal slice S_N^{t-1}).

4. When the outside of the first or last contact slice also contains non-contact slices, if a non-contact slice is located on the extension line of the actual contact line, the non-contact slice should also be considered. This is because although the non-contact slice is at the edge of the tooth, its posture

will change with the deflection of the adjacent contact slice (see Fig. 6a, nominal slice $S_N^{n_4}$).

5. The contacted element with the largest amount of deflection on each nominal slice is regarded as the Hertzian contact center of the nominal slice.

Based on the above definition of the nominal slice, an improved mesh stiffness model is proposed, as shown in Fig. 7. In the traditional slicing method, the total mesh stiffness is obtained through the superposition of the single tooth mesh stiffness, and the coupling effects between the deflections of the adjacent slice and the adjacent tooth are not considered, which will cause a large error in the calculation result of the total mesh stiffness. In this study, four correction coefficients, W_F^i, C_F, η, and λ, are introduced to consider the above-mentioned two coupling effects as in [9] and [10], respectively. Among them, W_F^i is the weighting factor of the slice S^i along the tooth width that considers the coupling effect between the deflections of the adjacent slice that is dependent on the helix angle and tooth width. C_F is a correction factor that offsets the decrease in the mesh stiffness caused by the weighting factor W_F^i. η and λ are the correction coefficients of the foundation stiffness and the foundation stiffness under double-tooth meshing duration, respectively. The above four correction coefficients are obtained through FEM, the calculation methods of W_F^i and C_F are given elsewhere [9], and the
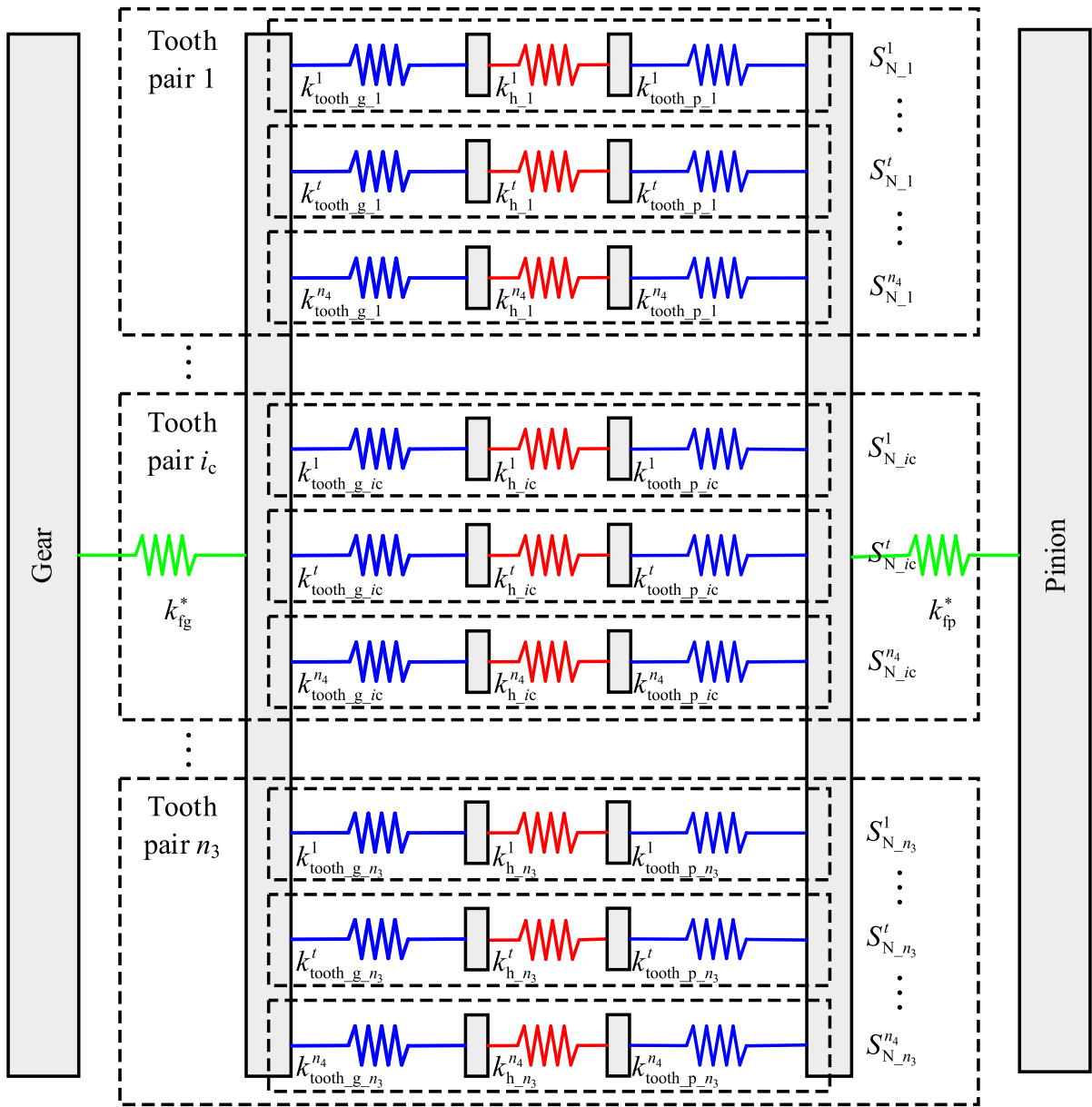
Fig. 7 Improved mesh stiffness model

calculation methods of η and λ are also given elsewhere [10]. Hence, the correction foundation stiffness in Fig. 7 (k_{fp}^* and k_{fg}^*) can be expressed as follows:

$$k_{\text{fp,g}}^* = \sum_{i=1}^{n_1} k_{\text{fp,g}}^{i*}, \tag{19}$$

where n_1 is the total number of slices along the tooth width, $k_{\text{fp,g}}^{i*}$ is the correction foundation stiffness of the

slice S^i, and subscripts p and g denote the pinion and the gear in the rest of paper, respectively. When slice S^i is located on the single-tooth meshing duration and the double-tooth meshing duration, $k_{\text{fp,g}}^{i*}$ can be expressed as Eq. (20) and Eq. (21), respectively:

$$k_{\text{fp,g}}^{i*} = \eta_{\text{p,g}} C_{\text{F}} W_{\text{F}}^i k_{\text{f1p,g}}^{ij}, \tag{20}$$

$$k_{\text{fp,g}}^{i*} = \lambda_{\text{p,g}} \eta_{\text{p,g}} C_F W_F^i \cdot \max\left(k_{\text{f1p,g}}^{ij}, k_{\text{f2p,g}}^{ij}\right), \tag{21}$$

where subscripts 1 and 2 in $k_{\text{f1p,g}}^{ij}$ and $k_{\text{f2p,g}}^{ij}$ denote the first and second tooth pairs in the mesh, respectively; and the superscript j denotes the index of the contact element on the slice S^i. In this study, each slice constituting the helical gear is regarded as a non-uniform cantilever beam (see Fig. 8). The stiffness considering the gear fillet-foundation deflection of the element j on slice S^i ($k_{\text{f1p,g}}^{ij}$ and $k_{\text{f2p,g}}^{ij}$) is given as follows [2, 18, 37, 38]:

$$\frac{1}{k_f^{ij}} = \frac{\cos^2 \beta_j}{B^i E} \left\{ L^* \left(\frac{u_f}{S_f}\right)^2 + M^* \left(\frac{u_f}{S_f}\right) + P^* \left(1 + Q^* \tan^2 \beta_j\right) \right\}, \tag{22}$$

where B^i is the width of the slice S^i; S_f and u_f are defined in Fig. 8. The method to calculate L^*, M^*, P^*, and Q^* is given elsewhere [13].

In Fig. 7, $k_{\text{tooth\_p,g\_}ic}^t$ denotes the tooth stiffness of the nominal slice $S_{\text{N\_}ic}^t$ on the tooth pair i_c. The tooth stiffness includes the tooth bending stiffness, shear stiffness, and the axial compressive stiffness, and $k_{\text{tooth\_p,g\_}ic}^t$ can be expressed as follows:

$$k_{\text{tooth\_p,g\_}ic}^t = \sum_{i=i_{\text{p,g}}-n_{\text{lp,g}}}^{i_{\text{p,g}}+n_{\text{np,g}}} \frac{C_F W_F^i}{\frac{1}{k_b^{ij}} + \frac{1}{k_s^{ij}} + \frac{1}{k_a^{ij}}}, \tag{23}$$

where the superscript t is the index of the nominal slice

$S_{\text{N\_}ic}^t$; i_{p} and i_{g} are the indices of the slices where the Hertzian contact center of the nominal slice S_{N}^t is located; n_{lp} and n_{lg} are half the number of uncontacted slices between the current and the last contacted slices, respectively; n_{np} and n_{ng} are half the number of uncontacted slices between the current and the next contacted slices, respectively; subscripts p and g represent the pinion and gear, respectively; and k_b^{ij}, k_s^{ij}, and k_a^{ij} are the bending stiffness, shear stiffness, and the axial compressive stiffness of the element j on slice S^i, respectively. It should be noted that if the slice S^i loses contact, the index j is obtained by interpolation. Based on the non-uniform cantilever beam model (see Fig. 8), k_b^{ij}, k_s^{ij}, and k_a^{ij} are given as follows [2, 15, 16]:

$$\frac{1}{k_b^{ij}} = \int_0^L \frac{\left(x \cos \beta_j - h \sin \beta_j\right)^2}{E I_x} dx, \tag{24}$$

$$\frac{1}{k_s^{ij}} = \int_0^L \frac{1.2 \cos^2 \beta_j}{G A_x} dx, \tag{25}$$

$$\frac{1}{k_a^{ij}} = \int_0^L \frac{\sin^2 \beta_j}{E A_x} dx, \tag{26}$$

where G and E are the shear and the Young's moduli, respectively, I_x is the area moment of inertia, A_x is the area of the section, x, dx, β_j, h, L, and h_x are shown in Fig. 8, and the Poisson's ratio is represented by υ. These parameters can be calculated as follows:
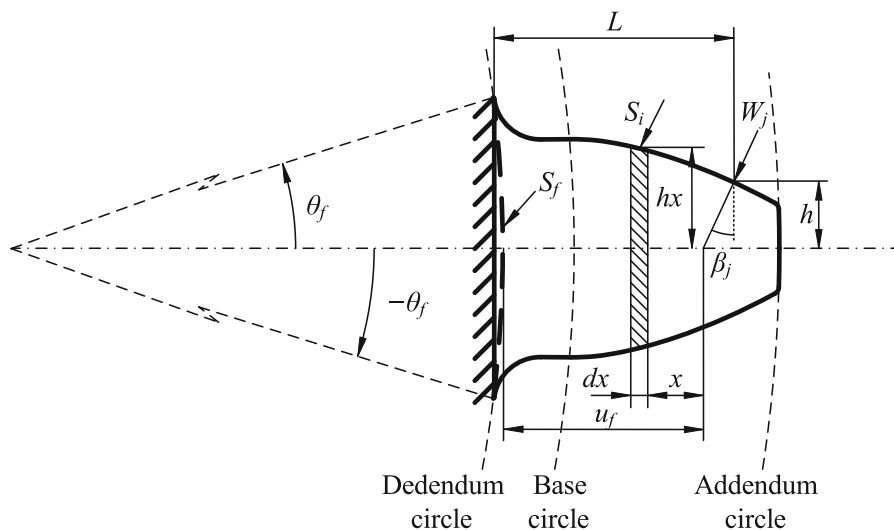

Fig. 8 Non-uniform cantilever beam

$$I_x = \frac{2h_x^3 B^i}{3n_1}, \tag{27}$$

$$A_x = \frac{2h_x B^i}{n_1}, \tag{28}$$

$$G = \frac{E}{2(1 + \upsilon)}. \tag{29}$$

According to previous publications [12, 39], the contact deflection is usually regarded as the local deflection. Hence, when calculating the contact stiffness of the nominal slice $S_{N\_ic}^t$, only the slice participating in contact is considered. The contact stiffness of the nominal slice $S_{N\_ic}^t$ on the tooth pair i_c can be calculated as follows [40]:

$$\frac{1}{k_{h\_ic}^t} = \frac{4(1 - \upsilon^2)}{\pi E B^i}. \tag{30}$$

According to the flowchart of the calculation of the TVMS (see Fig. 5), the gear is rotated clockwise to an output position and fixed, and the pinion is rotated counterclockwise by a smaller step to approach the gear until the load is balanced. Based on Fig. 7, the deflection and load compatibility conditions are given as follows:

$$\begin{cases} \delta_{fg} + \delta_{N\_1}^1 + \delta_{fp} = \delta_1^1 \\ \qquad\qquad\qquad \vdots \\ \delta_{fg} + \delta_{N\_ic}^t + \delta_{fp} = \delta_{i_c}^t \\ \qquad\qquad\qquad \vdots \\ \delta_{fg} + \delta_{N\_n_3}^{n_4} + \delta_{fp} = \delta_{n_3}^{n_4} \\ k_{fg}^* \delta_{fg} = \sum\limits_{i_c=1}^{n_3} \left[\sum\limits_{t=1}^{n_4} \delta_{N\_ic}^t \left(\dfrac{1}{1/k_{tooth\_g\_ic}^t + 1/k_{h\_ic}^t + 1/k_{tooth\_p\_ic}^t} \right) \right] \\ k_{fg}^* \delta_{fg} = k_{fp}^* \delta_{fp} \end{cases}, \tag{31}$$

where δ_{fp} and δ_{fg} are the foundation deflections of the pinion and gear, respectively; $\delta_{N\_ic}^t$ is the comprehensive deflection of the nominal slice, $S_{N\_ic}^t$, on the tooth pair i_c, including the bending, shear, axial compressive deflections, and the Hertzian contact deflection; and $\delta_{i_c}^t$ is the total deflection of the contact center of the nominal slice, $S_{N\_ic}^t$, which has been obtained by the geometric method in Sect. 2.2. In the initial stage of the iterative process, the total mesh force is not sufficient to balance the external load. The pinion continues to rotate, and the deflection of the contacted nominal slices increases until the difference

between the torque generated by the total mesh force and the rated output torque satisfies the requirements of the calculation accuracy, as shown in Fig. 5. The convergence condition is

$$k_{fg}^* \delta_{fg} r_{bg} - T_g < e, \tag{32}$$

where T_g and r_{bg} are the torque and the radius of the base circle of the gear, respectively.

Based on the mesh stiffness model in Fig. 7, the TVMS of the gear pair is expressed as follows:

$$k_{mesh} = \frac{1}{\dfrac{1}{k_{fg}^*} + \dfrac{1}{k_{fp}^*} + \dfrac{1}{\sum\limits_{i_c}^{n_3} \left[\sum\limits_{t=1}^{n_4} \dfrac{1}{1 / k_{tooth\_g\_ic}^t + 1 / k_{h\_ic}^t + 1 / k_{tooth\_p\_ic}^t} \right]}}. \tag{33}$$

3 Validation of proposed method

Because the spur gear is a unique helical gear ($\beta = 0$), the difference in the proposed method is that the discrete element (see Fig. 3a) is equivalent to a cylindrical surface rather than a helical arc surface. In this section, a spur gear pair and a helical gear pair, as shown in Table 1, were applied to the proposed method. The TVMSs calculated by the proposed method were compared with previously reported results [10, 19, 41] and the FEM results in [10, 41] to verify the effectiveness of the proposed method, as shown in Fig. 9.

In Fig. 9a, the TVMS calculated using the method proposed agreed well with the FEM result, and was better than the result calculated by Xie's method. The errors between the calculation results of the proposed method and the FEM results at positions A and B were 0.51% and 1.85%, respectively. This finding implies that the method is practical for spur gear pairs. The comparison of the TVMSs of the helical gear pair is shown in Fig. 9b. The mesh stiffness of the multi-tooth meshing region was obtained through the superposition of the single-tooth meshing stiffness in Wan's method, and the coupling effect between the deflections of the adjacent tooth was not considered, which causes the calculation results of the TVMS to be larger than the actual value. The variation trends of the TVMS curves in this study were consistent with the calculation result of Huangfu's method, and the

Table 1 Parameters of the gear pairs

	Spur gear pair			Helical gear pair	
	Pinion	Gear		Pinion	Gear
Number of teeth	60	60		40	40
Normal module (mm)	2	2		4	4
Helix angle (°)	–	–		10	10
Pressure angle (°)	20	20		20	20
Face width (mm)	20	20		30	30
Hub radius (mm)	25	25		30	30
Poisson's ratio	0.3	0.3		0.3	0.3
Young's modulus (N/mm^2)	2.068×10^5	2.068×10^5		2.12×10^5	2.12×10^5
Applied torque (Nm)	50			100	
Number of elements along tooth profile	100	100		100	100
Number of elements along tooth width	200	200		200	200
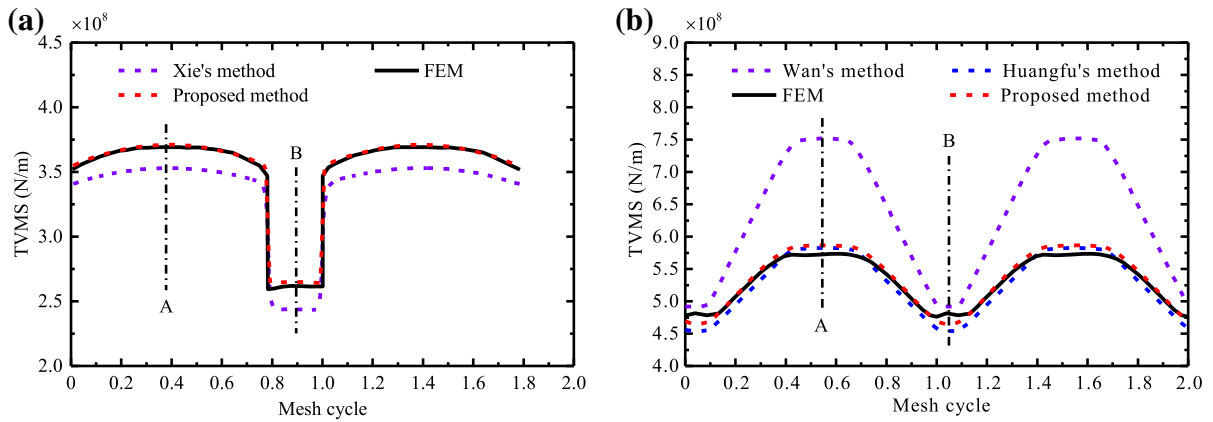
Fig. 9 TVMS and the number of contact pairs of **a** the spur and **b** helical gear pairs

TVMS calculated by the proposed method was closer to the FEM result than the result obtained by Huangfu's method in three-tooth meshing region (see position B in Fig. 9b). The errors between the calculation results of the proposed method and the FEM result at positions A and B in Fig. 9b were 2.29% and 2.57%, respectively. The above results show that the proposed method has good accuracy and is effective for both spur and helical gear pairs.

4 Results and discussions

In previous publications, the effects of many factors on the TVMS of helical gear pairs have been studied,

such as the gear parameters [25], tooth cracks [10, 25, 26], friction, and mesh misalignment [27]. In this section, the TVMSs of a helical gear pair at different accuracy grades were predicted, and the influence mechanisms of MEs, AEs, and TMs on the TVMS were investigated. The helical gear pair shown in Table 1 was used in this section.

4.1 Effect of manufacturing errors

To predict the TVMS of the helical gear pair under different accuracy grades, the gear precision parameters of the MEs were first obtained based on the ISO standard [36], as shown in Table 2. The single pitch deviation, total cumulative pitch deviation, total

profile deviation, total helix deviation, tooth thickness deviation, and base tangent length were considered. According to previously published works [5, 34, 35], the sine function usually simulates the cumulative pitch deviation, but it ignores the effect of the randomness of the pitch deviation on the contact state of the gear teeth. Therefore, the cumulative pitch deviation in this study was simulated by superposing a sine function and a random variable that obeys the normal distribution, and the remaining MEs were obtained through random functions on the basis of meeting the tolerance range requirements in Table 2. In addition, the TVMS is not only related to the MEs but also related to the size of the load. Normally, the TVMS is more sensitive to errors at light loads than at heavy loads. As the effect of load on the TVMS of helical gear pairs has been investigated previously [5], only TVMSs under a perfect tooth surface, grade 4, grade 5, and grade 6 when the output torque is 500 Nm, and TVMS under grade 4 when the output torque is 100 Nm were calculated in this study, as shown in Fig. 10.

In Fig. 10, the peak-to-peak values of the TVMS under a perfect tooth surface, grade 4, grade 5, and grade 6 when the output torque was 500 Nm were 1.2262×10^{8}, 1.1930×10^{8}, 1.1573×10^{8}, and 1.1567×10^{8} N/m, respectively. This shows that the MEs led to a peak-to-peak change of the TVMS. The mean values of the TVMS under a perfect tooth surface, grade 4, grade 5, and grade 6 when the output torque was 500 Nm were 5.3837×10^{8}, 5.2579×10^{8}, 5.1164×10^{8}, and 4.9603×10^{8} N/m, respectively, which decreased with the decrease in the gear accuracy grade. In addition, Fig. 10 also shows that the lower the gear accuracy grade was under the same load, the more severe the vibrations of the TVMS curve became, and the greater the

difference in waveform was. This occurred because the deviation range of the MEs increased as the gear accuracy grade decreased, while a larger deviation range was more likely to cause out-of-line meshing, the loss of contact of partial tooth pairs, and other abnormal contact statuses. Comparing the TVMS at different loads under grade 4, it can be found that the mean value of the TVMS when the output torque was 100 Nm (4.0986×10^{8} N/m) was much smaller than the mean value at 500 Nm, and the vibration of the TVMS curve was more severe when the output torque was 100 Nm. This occurred because the TVMS was not only related to the MEs but also related to the size of the load. However, 100 Nm was too small compared to the load capacity of this helical gear pair, and the sensitivity of the TVMS to the MEs increased at light loads because the load deflection of the tooth at light loads could not readily compensate for the gap between the tooth surfaces caused by the MEs. Thus, the accuracy grades affected not only the peak-to-peak and mean values of the TVMS but also its waveform. To reveal the influence mechanisms of MEs on the TVMS, different types of grade 4 MEs were applied using the presented method, and the calculation results of the TVMS are shown in Fig. 11. It is worth noting that the output torque was set to 100 Nm in the rest of this section to highlight the influence mechanism of MEs on the TVMS. When the helical gear pair was working under the rated load, the sensitivity of the TVMS to the MEs was reduced.

Figure 11 shows that the pitch and helix deviations were the main factors affecting the TVMS. When only the pitch deviations were considered, the TVMS curve underwent a step change at some positions, such as $\theta_1 = 0.9$ rad. Figure 12a shows the number of contact pairs when the pitch deviations were considered. When the TVMS curve underwent a step change, the

Table 2 Precision parameters of the helical gear pair

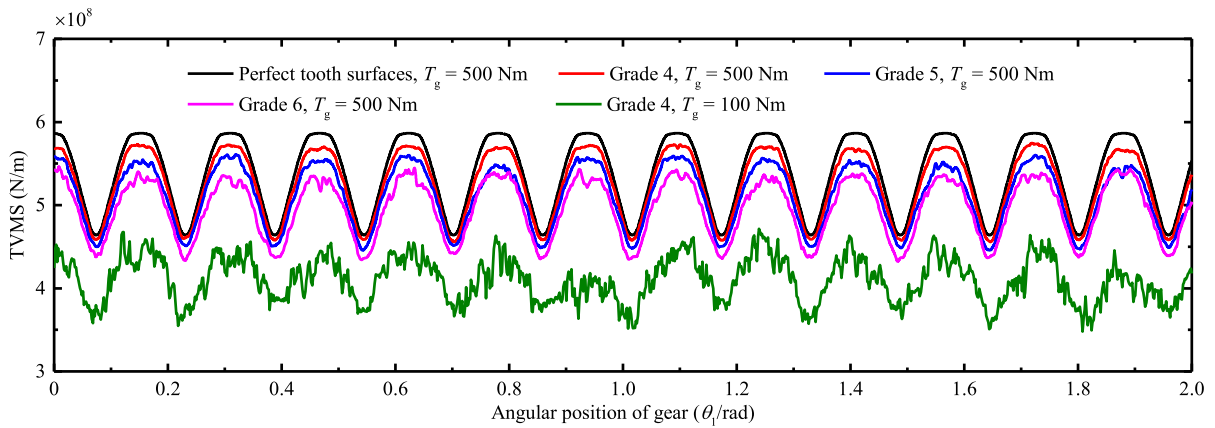| Precision parameters (Symbol/unit)	Grade 4	Grade 5	Grade 6
Single pitch deviation ($\pm f_{pt}$/μm)	5.0	7.0	10.0
Total cumulative pitch deviation (F_p/μm)	18.0	25.0	36.0
Total profile deviation (F_α/μm)	7.5	11.0	15.0
Total helix deviation (F_β/μm)	6.5	9.0	13.0
Tooth thickness deviation (E_s/mm)	$6.283^{-0.040}_{-0.079}$	$6.283^{-0.063}_{-0.126}$	$6.283^{-0.10}_{-0.20}$
Base tangent length (W_k/mm)	$55.479^{-0.037}_{-0.074}$	$55.479^{-0.059}_{-0.118}$	$55.479^{-0.094}_{-0.188}$
	($k = 5$)	($k = 5$)	($k = 5$)

Fig. 10 Prediction results of the TVMS under different accuracy grades
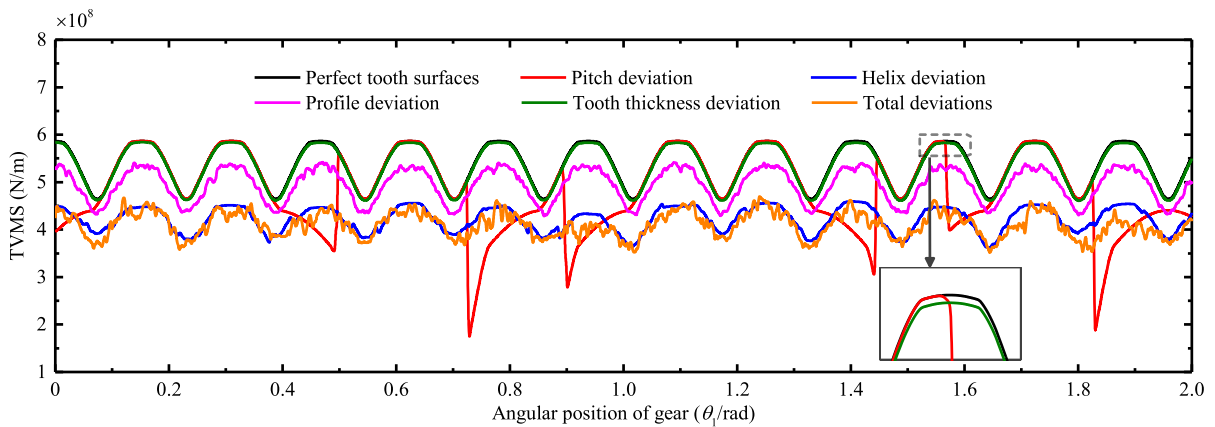

Fig. 11 Effects of different types of MEs on the TVMS

number of instantaneous contact pairs changed. This occurred because the pitch deviations of each tooth were different in this study, and the pitch deviations created a gap between the tooth pair involved in the meshing. When the gap was large enough and could not be compensated for by the deflection under the load of the neighboring teeth, the tooth pair lost contact. Therefore, the loss of contact of the tooth pairs due to the effect of the pitch deviations was the main reason for the step change of the TVMS curve. When only the helix deviations were considered, the peak-to-peak and mean values of the TVMS were greatly reduced. Figure 12b shows the comparison between the trajectory of the theoretical contact line and the actual contact line when helix deviations were considered with $\theta_1 = 1.5$ rad. Although all contact elements were located on the theoretical contact line, most of the slices lost contact, which was the reason

for the significant decrease in the peak-to-peak and mean values of the TVMS.

Figure 11 also shows that the profile and tooth thickness deviations had little effect on the TVMS. The profile deviations also led to a small decrease in the peak-to-peak and mean values of the TVMS curve and small fluctuations of the curve. Figure 12c shows that the contact elements when the profile deviations were considered were distributed on both sides of the theoretical contact line, which indicated that out-of-line meshing occurred. This is the cause of small fluctuations in TVMS curve. In addition, some slices lost contact because the tooth profile deviations of the elements were too large, which led to a decrease in the peak-to-peak and mean values of the TVMS curve. In Fig. 12d, the actual contact line when the tooth thickness deviations were considered completely coincided with the theoretical contact line. However,
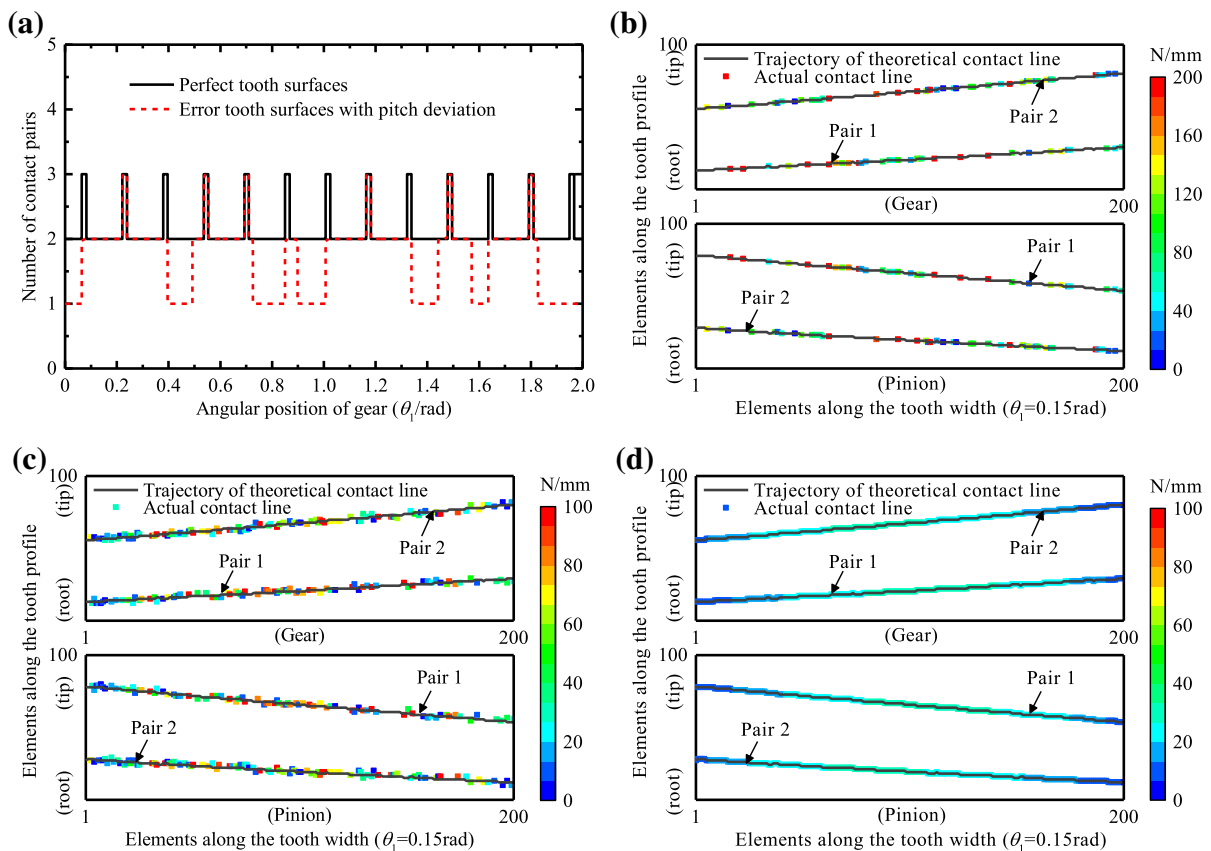
Fig. 12 Effects of different types of MEs on the tooth surface contact: **a** number of contact pairs considering pitch deviations, **b** contact line considering helix deviations, **c** contact line considering profile deviations, and **d** contact line considering tooth thickness deviations

as shown in the partial enlarged view in Fig. 11, the tooth thickness deviations caused a slight decrease in the peak-to-peak value of the TVMS curve, while the waveform was completely consistent with the curve when the tooth surfaces were perfect. This occurred because the tooth thickness deviations only changed the compliance of a single tooth, but the effect of the tooth thickness deviation on the compliance was slight. Consequently, the TVMS was mainly related to the pitch and helix deviations, and they should be properly controlled during the gear machining process to reduce the influence of MEs on the TVMS.

4.2 Effect of assembly errors

During the process of gear installation, AEs are inevitable, which leads to various abnormal meshing conditions, such as eccentric loads and out-of-line meshing. These meshing conditions will also have a non-negligible influence on the TVMS. According to the definition of AEs in Sect. 2.1, the AEs are represented by four parameters (Δx, Δy, φ, and γ) in this study. It is known that AEs can be divided into center distance deviations and misalignment deviations. Because Δx and Δy produce similar effects on the change of the center distance between two gears, only the effects of Δy, φ, and γ on TVMS were studied. Similarly, the output torque was set to 100 Nm in this section to highlight the influence mechanism of AEs on the TVMS. When the helical gear pair was working under the rated load, the sensitivity of the TVMS to the AEs was reduced.

Figure 13a shows the calculation results of the TVMS for different values of Δy. The TVMS at each position of the gear decreased as the center distance increased, and the greater the center distance deviations were, the greater the difference between it and the TVMS with perfect tooth surfaces was. In contrast,

the center distance deviations had little effect on the waveform of the TVMS. Figure 13b shows the actual contact line when $\Delta y = 0.4$ mm. The contact element on each slice moved to the tooth tip due to the increase in the center distance, while the compliance at the tooth tip was greater than that at the tooth root. Thus, the center distance deviations caused the contact line to move on the tooth surface, thereby changing the TVMS.

The effects of φ and γ (misalignment deviations) on the TVMS were investigated. Figure 14a shows the calculation results of the TVMS for different values of φ. The misalignment deviation φ not only affected the peak-to-peak and mean values of the TVMS but also changed its waveform. The greater the absolute value of φ was, the smaller the TVMS was. To reveal the reason for the decrease in the TVMS, Fig. 14b, c show the actual contact line when $\varphi = -0.02°$ and $0.02°$, respectively. When φ was negative, the right side of the tooth surface lost contact. In contrast, the left side of the tooth surface lost contact when φ was positive. Both conditions caused the actual contact line to be shorter than the theoretical contact line, thereby reducing the TVMS. In addition, the contact stress of the tooth surface when $\varphi = 0.02°$ was obtained according to Hertzian contact theory, as shown in Fig. 14d. The contact stress was mainly distributed on the right tooth surface, which was consistent with the results of Fig. 14c. These results unanimously indicated that an eccentric load occurred on the tooth surface due to the effect of φ.

The TVMSs for different values of γ are shown in Fig. 15a. When the absolute value of γ was small (0.01°), the peak-to-peak and mean values and waveform of the TVMS curve did not change significantly. As the absolute value of γ increased, the peak-to-peak and mean values of the TVMS curve decreased significantly. Compared with the results of the TVMS under the same misalignment deviation φ, the misalignment deviation γ had a smaller effect on the TVMS. Figure 15b shows the actual contact line when $\gamma = 0.02°$. It can be found that the misalignment deviation γ also caused part of the tooth surface to lose contact. Compared to Fig. 14c, the misalignment deviation φ caused more elements to lose contact than γ under the same value of φ and γ. Therefore, ensuring the assembly accuracy of φ during the process of gear installation can significantly reduce the influence of AEs on the TVMS compared with Δy and γ.

4.3 Effect of tooth modifications

In engineering practice, profile modification is widely used to decrease the shock, vibrations, and noise of gear transmission systems, and lead crowning is used to improve the uneven distribution of the load on the contact line. However, the different amounts and lengths of TMs under the same load will cause the contact state between the two gears to change. For example, excessive modification will lead to a loss of contact of the tooth pairs located in the mesh-in and mesh-out regions, which will cause a significant
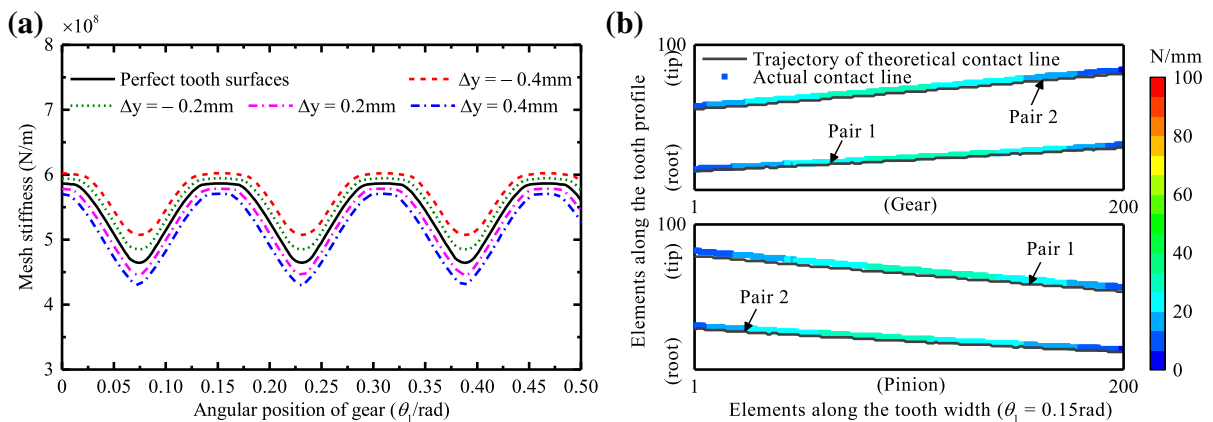

Fig. 13 Results of different center distance deviations: **a** TVMS, and **b** contact line considering the center distance deviations ($\Delta y = 0.4$ mm)
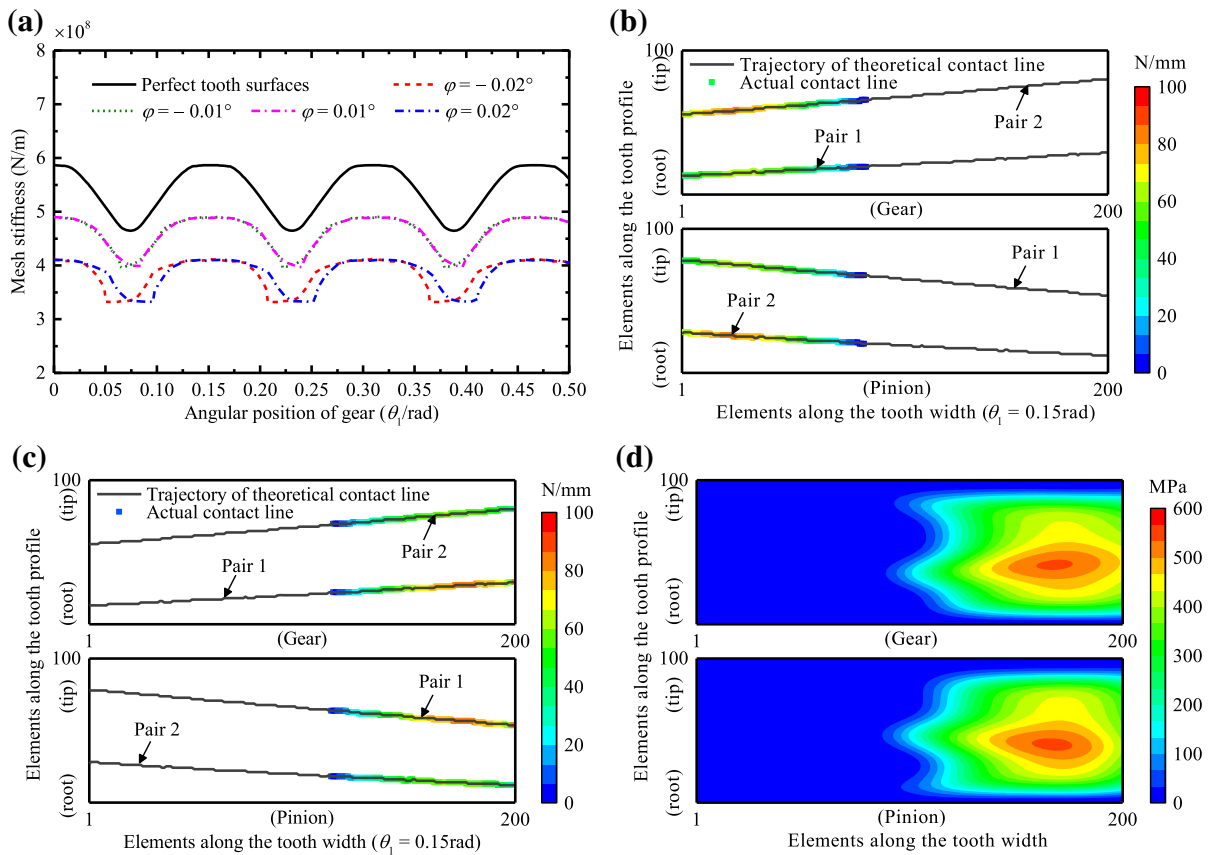
(a)

(b)

(c)

(d)

Fig. 14 Results of different misalignment deviations (φ): **a** TVMS, **b** contact line when $\varphi = -0.02°$, **c** contact line when $\varphi = 0.02°$, and **d** contact stress when $\varphi = 0.02°$
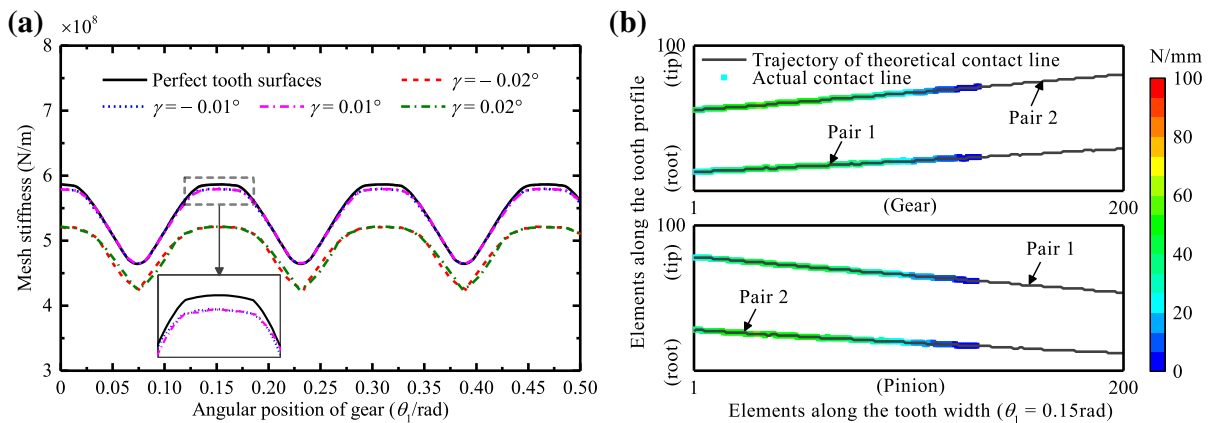
(a)

(b)

Fig. 15 Results of different misalignment deviations (γ): **a** TVMS and **b** contact line when $\gamma = 0.02°$

decrease in the TVMS and cause adverse effects on the gear transmission system. Thus, the influence of TMs on the TVMS cannot be ignored. In this section, the output torque is set to 500 Nm.

On the profile modification side, Fig. 16a, b show the TVMS and the number of contact pairs with different modification amounts under the same modification length ($L_1 = 1.6$ mm), respectively. This

shows that the range of the three-tooth contact region and the TVMS did not change when $C_a = 3$ μm. When $C_a = 8$ μm, the range of the three-tooth contact region was slightly reduced, and the slope of the TVMS curve near the peak decreased. This indicated that most slices along the tooth width remained in contact under the influence of the load deflection, and only a few slices were out of contact. Although the material removal on the tooth surface due to the profile modification will increase the compliance of the tooth, its influence can be ignored when $C_a = 8$ μm. However, as the amount of profile modification continued to increase, the three-tooth contact region became smaller or even suddenly changed to the single-tooth contact region (see Fig. 16b, $C_a = 15$ μm). This indicates that the excessive modification led to the loss of contact of the tooth pairs located in the mesh-in and mesh-out regions. The greater the amount of modification was, the smaller the range of the multi-tooth contact region became. In addition, the TVMS

also decreased with the further increase of the profile modification amount. For example, although there were two teeth in contact before and after the modification when $\theta_1 = 0.1$ rad, the TVMS was reduced by about 3.67% ($C_a = 15$ μm). Figure 16c, d show the actual contact lines under different amounts of modification ($C_a = 8$ and 15 μm) when $\theta_1 = 0.15$ rad. This shows that when the modification amount was too large, the load deflection of the tooth was not sufficient to compensate for the gap between the meshing slices due to the modification. Therefore, the elements near the tooth tip lost contact. The greater the amount of modification was, the more elements lost contact.

Figure 17a, b show the TVMS and the number of contact pairs with different modification lengths under the same modification amount ($C_a = 15$ μm). When $L_1 = 0.8$ mm, the TVMS was almost the same as the TVMS under the perfect tooth surfaces.
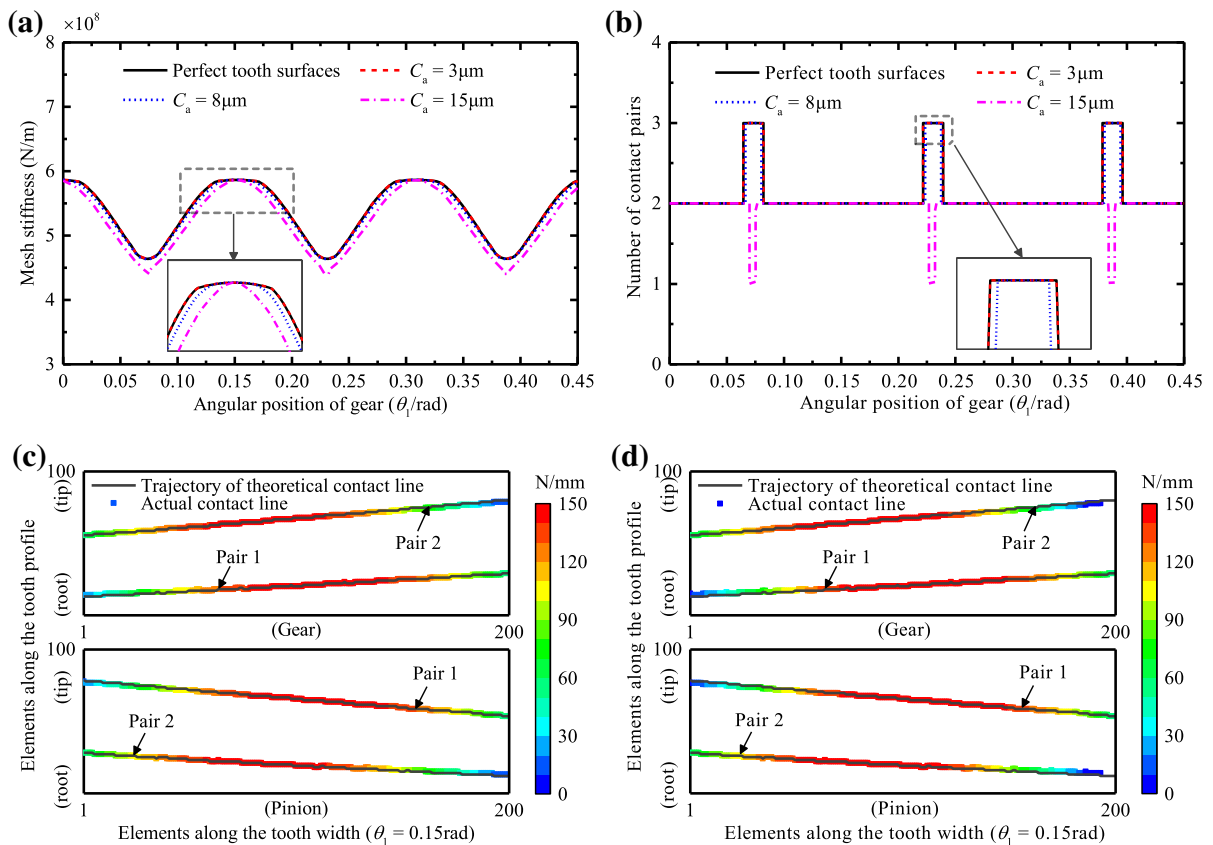

Fig. 16 Results of different profile modification amounts ($L_1 = 1.6$ mm): **a** TVMS, **b** number of contact pairs, **c** contact line when $C_a = 8$ μm, and **d** contact line when $C_a = 15$ μm

Similarly, as the profile modification length increased, the three-tooth contact region became smaller or even suddenly changed to the single-tooth contact region (see Fig. 17b, L_1 = 1.6 mm and L_1 = 2.4 mm). In addition, a step change occurred at the trough of the TVMS curve when L_1 = 1.6 and 2.4 mm. This was caused by the loss of contact of the tooth pairs located in the mesh-in and mesh-out regions (see Fig. 17b). The sudden change in the number of contact pairs resulted in a step change in the TVMS. Figure 17a also shows that as the length of the profile modification increased, the TVMS decreased, while the TVMS was almost the same in the single-tooth contact region, such as at θ_1 = 0.225 rad. This occurred because a parabola was used as the profile modification curve, and when the modification length increased, the range of the loss of contact elements near the tooth tip became larger (see Fig. 17c, d). As the instantaneous contact line of the contacting tooth pair was outside the area of the profile modification on

the tooth surface when θ_1 = 0.225 rad, the TMVS was not affected, but the range of the single-tooth contact region became larger with the increase in the modification length. In conclusion, in the design process of the gear, the amount and length of the profile modification should be reasonably selected based on the operating conditions to avoid the adverse influence of profile modifications on the TVMS.

Figure 18a, b show the TVMS and the number of contact pairs for different modification amounts of the lead crowning, respectively. This indicated that the TVMS and the range of the multi-tooth contact region remained unchanged when the modification amount of the lead crowning was within a certain range (e.g., C_b = 3 μm). However, when the modification amount exceeded this range, the TVMS decreased with the increase in the modification amount (e.g., C_b = 8 μm and C_b = 15 μm). There were two main reasons for the decrease in the TVMS. On the one hand, the lead crowning increased the initial gap between the mesh
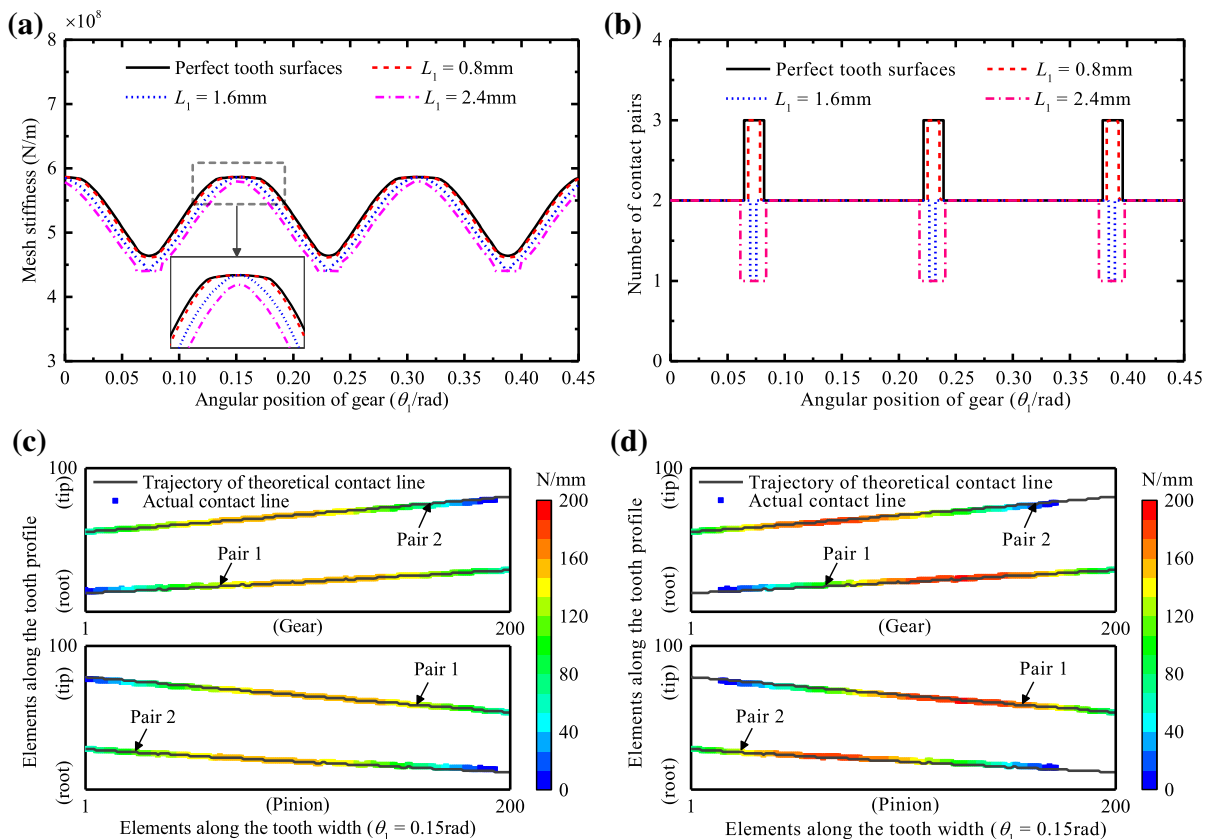

Fig. 17 Results of different profile modification lengths (C_a = 15 μm): **a** TVMS, **b** number of contact pairs, **c** contact line when L_1 = 1.6 mm, and **d** contact line when L_1 = 2.4 mm
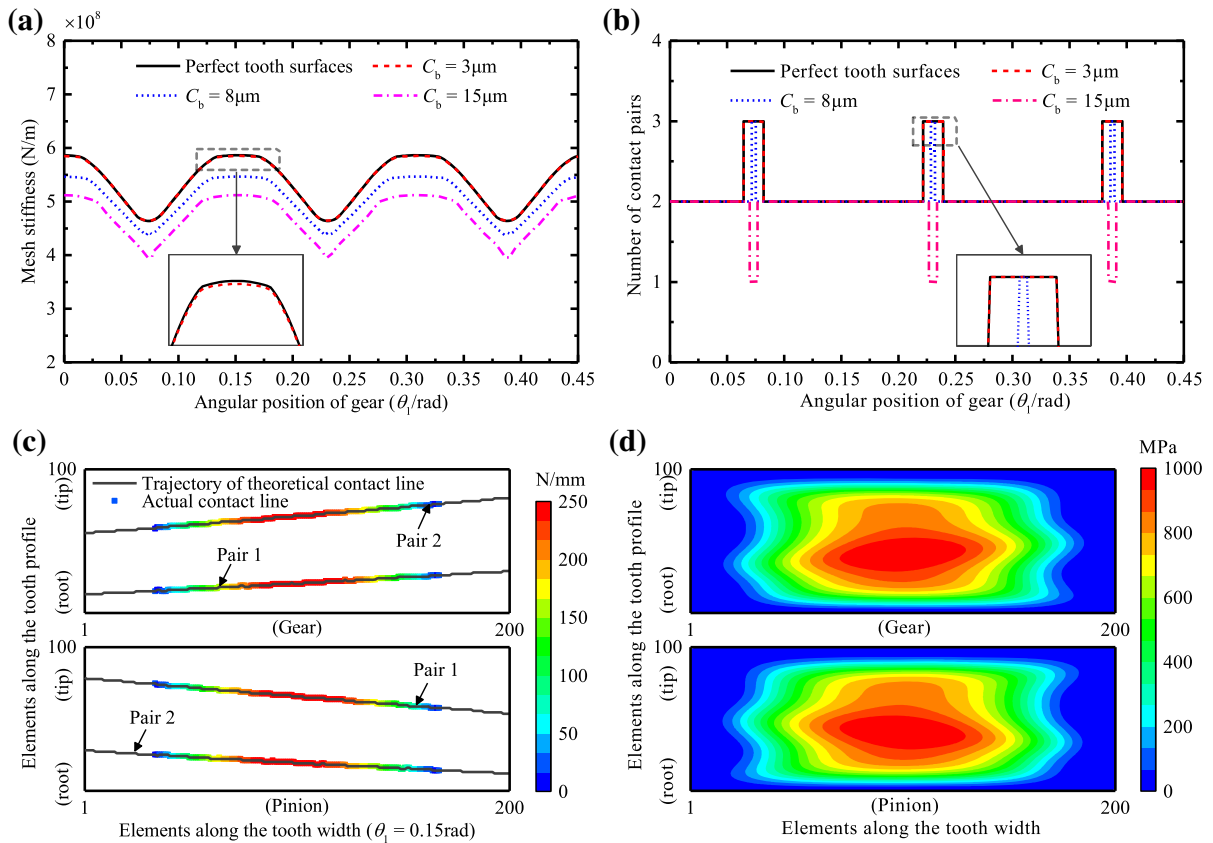
Fig. 18 Results of different amounts of lead crowning: **a** TVMS, **b** number of contact pairs, **c** contact line when $C_b = 8$ μm, and **d** contact stress when $C_b = 8$ μm

slices on the tooth surface, resulting in the loss of contact of the tooth pairs when the gap could not be compensated for by the tooth load deflection (see Fig. 18b). The range of the multi-tooth contact region also became smaller as the modification amount increased. On the other hand, although the number of contact pairs did not change when $\theta_1 = 0.15$ rad, the elements near the two sides of the tooth surface lost contact (see Fig. 18c), which caused the instantaneous contact line to become shorter. This was the main reason for the decrease in the TVMS due to the lead crowning. In addition, Fig. 18d shows the distribution of the contact stress on the tooth surface. It also shows that the contact region moved to the center of the tooth surface, which indicated that the lead crowning was helpful for improving the load distribution on the tooth surface.

5 Conclusions

A novel calculation method of the TVMS of helical gear pairs was proposed in this study, which was shown to be effective for both helical and spur gear pairs. The influence of some abnormal meshing phenomena, such as the loss of contact of tooth pairs, out-of-line meshing, and eccentric loads, on the TVMS was considered in the proposed method, and it has the capability of predicting the TVMS based on the different gear accuracy grades or the measurement coordinates of the tooth surface. Based on this method, the relationship between the MEs, AEs, TMs, and TVMS was revealed, and the sensitivity of the TVMS to different types of deviations was analyzed. The main conclusions are as follows:

1. The MEs affected not only the peak-to-peak and mean values of the TVMS but also its waveform. Furthermore, the pitch and helix deviations were

the main factors affecting the TVMS. The pitch deviations caused contact loss of partial tooth pairs, which caused the TVMS curve to produce a step change. The helix deviations caused the contact loss of partial slices along the contact line, thereby reducing the TVMS. In addition, out-of-line meshing occurred due to the influence of the profile deviations, and the tooth thickness deviations reduced the stiffness of the gear tooth. These two deviations had little effect on the TVMS.

2. For the AEs, the misalignment deviation φ caused the gear to be under an eccentric load, which greatly reduced the peak-to-peak and mean values of the TVMS. Compared to the misalignment deviation φ, the misalignment deviation γ had little influence on the TVMS. The center distance deviation changed the position of the contact line on the tooth surface, thereby affecting the mean value of the TVMS.

3. The profile modification caused contact loss of the elements near the tooth tip and reduced the range of the multi-tooth contact region, thereby reducing the mean value of the TVMS and even causing a step change in the TVMS curve. In the design process of the gear, the amount and length of the profile modification should be reasonably selected based on the operating conditions to avoid the adverse effects of the profile modifications on the TVMS. The lead crowning caused the contact region to move to the center of the tooth surface, and the length of its actual contact line decreased, which resulted in a reduction in the mean value of the TVMS.

The proposed method is expected to be used for the following three applications: (1) predicting the TVMS based on the tooth surfaces with errors generated by the gear accuracy grade or the measurement coordinates of the tooth surface, (2) reasonably controlling and optimizing the MEs, AEs, and parameters of the TMs to reduce the influence of error factors on the TMVS excitation, and (3) providing accurate TVMS excitations for the dynamic analysis of the gear transmission system instead of relying on the traditional method using approximate curves. Consequently, the proposed method is of great significance to the vibration and noise control of gear transmission systems.

References

1. Chen Z, Zhou Z, Zhai W, Wang K (2020) Improved analytical calculation model of spur gear mesh excitations with tooth profile deviations. Mech Mach Theory 149:103838
2. Chen Z, Shao Y (2011) Dynamic simulation of spur gear with tooth root crack propagating along tooth width and crack depth. Eng Fail Anal 18:2149–2164
3. Pimsarn M, Kazerounian K (2002) Efficient evaluation of spur gear tooth mesh load using pseudo-interference stiffness estimation method. Mech Mach Theory 37:769–786
4. Wang J, Howard I (2004) The torsional stiffness of involute spur gears. Proc IMechE Part C J Mech Eng Sci 218:131–142
5. Yuan B, Chang S, Liu G, Wu L (2018) Quasi-static and dynamic behaviors of helical gear system with manufacturing errors. Chin J Mech Eng 31:30
6. Ma H, Yang J, Song R, Zhang S, Wen B (2014) Effects of tip relief on vibration responses of a geared rotor system. Proc IMechE Part C J Mech Eng Sci 228:1132–1154
7. Shao Y, Chen Z, Wang S (2009) Simulation of spur gear pair with faults using FEA. In: ICROS-SICE international joint conference, Fukuoka, Japan, pp 2607−2610
8. Cooley CG, Liu C, Dai X, Parker RG (2016) Gear tooth mesh stiffness: a comparison of calculation approaches. Mech Mach Theory 105:540–553
9. Yu W, Mechefske CK (2019) A new model for the single mesh stiffness calculation of helical gears using the slicing principle. Iran J Sci Technol Trans Mech Eng 43:503–515
10. Huangfu Y, Chen K, Ma H, Che L, Li Z, Wen B (2019) Deformation and meshing stiffness analysis of cracked helical gear pairs. Eng Fail Anal 95:30–46
11. Cornell RW (1981) Compliance and stress sensitivity of spur gear teeth. ASME J Mech Des 103:447–459
12. Weber C (1949) The deformation of loaded gears and the effect on their load carrying capacity. Sponsored research (Germany). British Department of Science and Research, Report No. 3
13. Sainsot P, Velex P, Duverger O (2004) Contribution of gear body to tooth deflections: a new bidimensional analytical formula. ASME J Mech Des 126:748–752
14. Chen ZG, Zhang J, Zhai WM, Wang YW, Liu JX (2017) Improved analytical methods for calculation of gear tooth fillet-foundation stiffness with tooth root crack. Eng Fail Anal 82:72–81
15. Yang DCH, Lin JY (1987) Hertzian damping, tooth friction and bending elasticity in gear impact dynamics. J Mech Trans Automat Des 109:189–196

16. Tian XH (2004) Dynamic simulation for system response of gearbox including localized gear faults. M.S. thesis, University of Alberta, Canada

17. Wu S, Zuo MJ, Parey A (2008) Simulation of spur gear dynamics and estimation of fault growth. J Sound Vib 317:608–624

18. Chaari F, Fakhfakh T, Haddar M (2009) Analytical modelling of spur gear tooth crack and influence on gearmesh stiffness. Eur J Mech A/Solids 28:461–468

19. Wan Z, Cao H, Zi Y, He W, He Z (2014) An improved time-varying mesh stiffness algorithm and dynamic modeling of gear-rotor system with tooth root crack. Eng Fail Anal 42:157–177

20. Chen Z, Shao Y (2013) Mesh stiffness calculation of a spur gear pair with tooth profile modification and tooth root crack. Mech Mach Theory 62:63–74

21. Kahraman A, Blankenship GW (1999) Effect of involute contact ratio on spur gear dynamics. ASME J Mech Des 121:112–118

22. Lin J, Parker RG (2002) Planetary gear parametric instability caused by mesh stiffness variation. J Sound Vib 249:129–145

23. Lin J, Parker RG (2002) Mesh stiffness variation instabilities in two-stage gear systems. J Vib Acoust 124:68–76

24. Wang Q, Zhang Y (2015) A model for analyzing stiffness and stress in a helical gear pair with tooth profile errors. J Vib Control 23:272–289

25. Wan Z, Cao H, Zi Y, He W, Chen Y (2015) Mesh stiffness calculation using an accumulated integral potential energy method and dynamic analysis of helical gears. Mech Mach Theory 92:447–463

26. Jiang H, Liu F (2020) Mesh stiffness modelling and dynamic simulation of helical gears with tooth crack propagation. Meccanica 55:1215–1236

27. Han L, Xu L, Qi H (2017) Influences of friction and mesh misalignment on time-varying mesh stiffness of helical gears. J Mech Sci Technol 31:3121–3130

28. Feng M, Ma H, Li Z, Wang Q, Wen B (2018) An improved analytical method for calculating time-varying mesh stiffness of helical gears. Meccanica 53:1131–1145

29. Marques P, Martins R, Seabra J (2017) Analytical load sharing and mesh stiffness model for spur/helical and internal/external gears. Mech Mach Theory 113:126–140

30. Cao X, Deng X, Wei B (2018) A novel method for gear tooth contact analysis and experimental validation. Mech Mach Theory 126:1–13

31. Ma H, Zeng J, Feng R, Pang X, Wen B (2016) An improved analytical method for mesh stiffness calculation of spur gears with tip relief. Mech Mach Theory 98:64–80

32. Chen K, Huangfu Y, Ma H, Xu Z, Li X, Wen B (2019) Calculation of mesh stiffness of spur gears considering complex foundation types and crack propagation paths. Mech Syst Signal Process 130:273–292

33. Kurokawa S, Ariura Y, Ohtahara M (1996) Transmission errors of cylindrical gears under load-influence of tooth profile modification and tooth deflection. In: Proceedings of 7th ASME international power transmission and gearing conference, San Diego, USA, pp 213−217

34. Hu Z, Tang J, Zhong J, Chen S, Yan H (2016) Effects of tooth profile modification on dynamic responses of a high gear-totor-bearing system. Mech Syst Signal Process 76–77:294–318

35. Fernández-del-Rincón A, Iglesias M, de-Juan A, Diez-Ibarbia A, García P, Viadero F (2016) Gear transmission dynamics: Effects of index and run out errors. Appl Acoust 108:63–83

36. ISO 1328/1 (2013) Cylindrical gears-ISO system of flank tolerance classification-part 1: definitions and allowable values of deviations relevant to flanks of gear teeth, pp 1−50

37. Chaari F, Baccar W, Abbes MS, Haddar M (2008) Effect of spalling or tooth breakage on gearmesh stiffness and dynamic response of a one-stage spur gear transmission. Eur J Mech A/solids 27:691–705

38. Wang J (2003) Numerical and experimental analysis of spur gears in mesh. PhD thesis, Curtin University of Technology, Australia

39. Ajmi M, Velex P (2005) A model for simulating the quasi-static and dynamic behaviour of solid wide-faced spur and helical gears. Mech Mach Theory 40:173–190

40. Yang DCH, Sun ZS (1985) A rotary model for spur gear dynamics. J Mech Trans Automat Des 107:529–535

41. Xie C, Hua L, Han X, Lan J, Wan X, Xiong X (2018) Analytical formulas for gear body-induced tooth deflections of spur gears considering structure coupling effect. Int J Mech Sci 148:174–190